

## Supporting Information

---

### **Half-substituted fluorocycloparaphenylenes with high symmetry: Synthesis, properties and derivatization to densely substituted carbon nanorings**

Hiroki Shudo<sup>1</sup>, Motonobu Kuwayama<sup>2</sup>, Yasutomo Segawa<sup>2,3,4</sup>, Akiko Yagi<sup>1,5</sup>,  
and Kenichiro Itami<sup>1,2,5,\*</sup>

<sup>1</sup> Department of Chemistry, Graduate School of Science, Nagoya University, Nagoya  
464-8602, Japan

<sup>2</sup> JST, ERATO, Itami Molecular Nanocarbon Project, Nagoya University, Nagoya 464-  
8602, Japan

<sup>3</sup> Institute for Molecular Science, Myodaiji, Okazaki 444-8787, Japan

<sup>4</sup> The Graduate University for Advanced Studies, SOKENDAI, Myodaiji, Okazaki, 444-  
8787, Japan

<sup>5</sup> Institute of Transformative Bio-Molecules (WPI-ITbM), Nagoya University, Nagoya  
464-8602, Japan

\*E-mail: itami@chem.nagoya-u.ac.jp (K.I.)

---

### Table of Contents

1. Materials and methods	S2
2. Experimental section	S3–S6
3. Synthesis and purification	S7
4. X-ray crystallography	S8–S10
5. Photophysical measurements	S11–S13
6. Electrochemical measurements	S14
7. Computational studies	S15–S22
8. NMR spectra of <b>1</b> , <b>2</b> , <b>4</b> , and <b>5</b>	S24–S36
9. HRMS spectra of <b>1</b> , <b>2</b> , and <b>5</b>	S37–S38
10. References	S39

## 1. Materials and methods

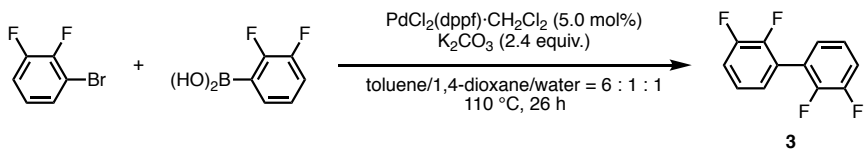
Unless otherwise noted, all reactants or reagents including dry solvents were obtained from commercial suppliers and used as received. Unless otherwise noted, all reactions were performed with dry solvents under an atmosphere of nitrogen in dried glassware using standard vacuum-line techniques. All work-up and purification procedures were carried out with reagent-grade solvents in air.

Analytical thin-layer chromatography (TLC) was performed using Wako silica gel 70 F<sub>254</sub> coated plates (0.25 mm); detection with UV light. Flash column chromatography was performed with E. Kanto silica gel 60 N (spherical, neutral, 40–100 µm). Preparative thin-layer chromatography (PTLC) was performed using Wakogel® B5-F silica coated plates (0.75 mm) prepared in our laboratory. The developed chromatogram was analyzed by a UV lamp (254 nm). Recycling preparative gel permeation chromatography (GPC) was performed with a JAI LC-9260II NEXT instrument equipped with JAIGEL-2HR-40 columns (40 mm I.D. × 600 mm × 2) using chloroform as an eluent.

The high-resolution mass spectra (HRMS) were obtained from a JEOL MS-T100TD (DART MS) and JEOL JMS-S3000 SpiralTOF (LDI-TOF MS). Nuclear magnetic resonance (NMR) spectra were recorded on a JEOL JNM-ECA-600 (<sup>1</sup>H 600 MHz, <sup>19</sup>F 565 MHz and <sup>13</sup>C{<sup>1</sup>H} 150 MHz) and JEOL JNM-ECZ-400 (<sup>1</sup>H{<sup>19</sup>F} 400 MHz, <sup>13</sup>C{<sup>1</sup>H,<sup>19</sup>F} 100 MHz) spectrometer. Chemical shifts for <sup>1</sup>H NMR are expressed in parts per million (ppm) relative to CHCl<sub>3</sub> ( $\delta$  7.26 ppm) or DMSO ( $\delta$  2.50 ppm). Chemical shifts for <sup>19</sup>F NMR are expressed in ppm relative to hexafluorobenzene (C<sub>6</sub>F<sub>6</sub>:  $\delta$  –164.9 ppm). Chemical shifts for <sup>13</sup>C{<sup>1</sup>H,<sup>19</sup>F} and <sup>13</sup>C{<sup>19</sup>F} NMR are expressed in ppm relative to CDCl<sub>3</sub> ( $\delta$  77.16 ppm) or tetramethylsilane ( $\delta$  0.00 ppm). Data are reported as follows: chemical shift, multiplicity (s = singlet, d = doublet, dd = doublet of doublets, m = multiplet, br = broad signal), and integration.

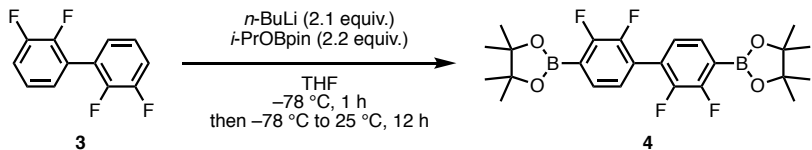
## 2. Experimental section

### Synthesis of 2,3,2',3'-tetrafluorobiphenyl (3)



To a 500-mL two-neck round-bottom flask containing a magnetic stirring bar were added 1-bromo-2,3-difluorobenzene (19.5 mL, 173 mmol), (2,3-difluorophenyl)boronic acid (31.7 g, 201 mmol), dichloro[1,1'-bis(diphenylphosphino)ferrocene]palladium(II) dichloromethane adduct (PdCl<sub>2</sub>(dppf)·CH<sub>2</sub>Cl<sub>2</sub>, 7.05 g, 8.63 mmol), potassium carbonate (57.5 g, 416 mmol), toluene (240 mL), 1,4-dioxane (40 mL), and water (40 mL). The reaction mixture was stirred at 110 °C for 26 h. After cooling the reaction mixture to room temperature, the organic layer was extracted with ethyl acetate, dried over Na<sub>2</sub>SO<sub>4</sub>, and then evaporated *in vacuo*. The crude material was purified by silica gel column chromatography (eluent: hexane) to afford 2,3,2',3'-tetrafluorobiphenyl (**3**) (27.1 g, 70%) as a colorless solid. The data was consistent with the reference.<sup>[S1]</sup>

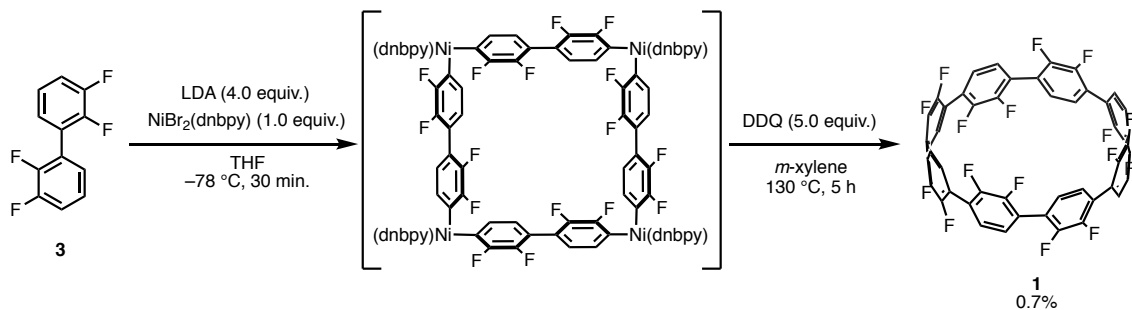
### Synthesis of 2,2'-(2,2',3,3'-tetrafluoro-[1,1'-biphenyl]-4,4'-diyl)bis(4,4,5,5-tetramethyl-1,3,2-dioxaborolane) (4)



To a 100-mL two-neck round-bottom flask containing a magnetic stirring bar were added **3** (454 mg, 2.00 mmol) and tetrahydrofuran (THF, 20 mL). A hexane solution of *n*-butyllithium (1.6 M, 2.80 mL, 4.2 mmol) was added to the flask at -78 °C, and the reaction mixture was stirred at -78 °C for 1 h. Then, 2-isopropoxy-4,4,5,5-tetramethyl-1,3,2-dioxaborolane (*i*-PrOBpin, 0.90 mL, 4.4 mmol) was added at -78 °C, and the resulting mixture was stirred at 25 °C for 12 h. The reaction mixture was quenched by the addition of water (10 mL). The organic layer was extracted with ethyl acetate, dried over Na<sub>2</sub>SO<sub>4</sub>, and then evaporated *in vacuo*. The crude material was purified by GPC column chromatography (eluent: chloroform) to afford 2,2'-(2,2',3,3'-tetrafluoro-[1,1'-biphenyl]-4,4'-diyl)bis(4,4,5,5-tetramethyl-1,3,2-dioxaborolane) (**4**) (262 mg, 27%) as a colorless solid.

<sup>1</sup>H NMR (600 MHz, CDCl<sub>3</sub>) δ 7.53 (dd, *J* = 7.7, 5.0 Hz, 2H), 7.07–7.10 (m, 2H), 1.37 (s, 24H); <sup>13</sup>C NMR (150 MHz, CDCl<sub>3</sub>) δ 155.01 (dd, *J*<sub>CF</sub> = 253.6, 10.8 Hz), 147.97 (dd, *J*<sub>CF</sub> = 254.3, 15.9 Hz), 130.68 (d, *J*<sub>CF</sub> = 4.3 Hz), 127.28 (d, *J*<sub>CF</sub> = 10.1 Hz), 125.52 (s), 118.86 (br), 84.36 (s), 24.82 (s); HRMS (DART MS) *m/z* calcd for C<sub>24</sub>H<sub>28</sub>B<sub>2</sub>F<sub>4</sub>O<sub>4</sub> [M]<sup>+</sup>: 478.21098, found: 478.21210.

## Synthesis of 1

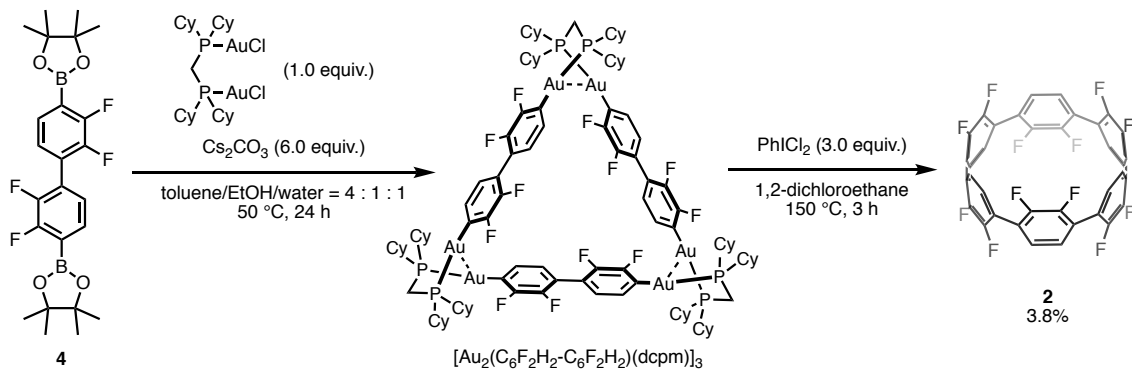


To a 2-L two-neck round-bottom flask containing a magnetic stirring bar were added 4,4'-dinonyl-2,2'-bipyridyl (dnbp), 24.5 g, 60.0 mmol,  $\text{NiBr}_2$  (13.3 g, 60.6 mmol), and dry THF (1.0 L). The reaction mixture was stirred at  $80^\circ\text{C}$  for 24 h. After cooling the reaction mixture to room temperature, the suspension was filtrated and the resulting filtrate was evaporated *in vacuo* to obtain  $\text{NiBr}_2(\text{dnbp})$  as a green solid (37.6 g), which was used without further purification.<sup>[S3]</sup>

To a 200-mL two-neck round-bottomed flask containing a magnetic stirring bar were added 2,3,2',3'-tetrafluorobiphenyl (1.13 g, 5.00 mmol),  $\text{NiBr}_2(\text{dnbp})$  (3.14 g, 5.00 mmol), and dry THF (66 mL). A 2.0 M solution of lithium diisopropylamide (LDA) in THF (10.0 mL, 20.0 mmol) was added to the flask at  $-78^\circ\text{C}$ . After the reaction mixture was stirred for 30 min, volatile solvents were evaporated *in vacuo*. The flask was filled by nitrogen gas, and 2,3-dichloro-5,6-dicyano-*p*-benzoquinone (DDQ, 5.68 g, 25.0 mmol) and degassed *m*-xylene (100 mL) were added to the flask. The reaction mixture was stirred at  $130^\circ\text{C}$  for 5 h. After cooling the reaction mixture to room temperature, the reaction mixture was filtrated through Celite® with chloroform (1.0 L), and the resulting filtrate was evaporated *in vacuo*. The crude product of two batches was combined and purified by silica gel column chromatography (eluent: hexane/chloroform = 3:1 (4 L) to 2:1 (3 L), and then 1:1 (1 L), and fractions which have light blue fluorescence by UV lamp at 365 nm were collected (see Supplementary Fig. S1)) and then GPC (the crude solid (ca.120 mg) was dissolved in 20 mL chloroform, filtered with a Hydrophilic PTFE 0.45  $\mu\text{m}$  Membrane filter (Millex-LCR 13 mm), and each 10 mL of resulting solution was injected to the GPC. Fractions were collected at the third cycle (see Supplementary Fig. S2). to afford 1 (14.9 mg, 0.7%) as a white solid.

$^1\text{H}$  NMR (600 MHz,  $\text{CDCl}_3$ )  $\delta$  7.05 (s, 16H);  $^{19}\text{F}$  NMR (565 MHz,  $\text{CDCl}_3$ )  $\delta$  -140.58 (br, 16F);  $^{13}\text{C}\{\text{H}\}$  NMR (150 MHz,  $\text{CDCl}_3$ )  $\delta$  149.21 (dd,  $J_{\text{CF}} = 256.5, 13.7$  Hz), 126.50 (s), 125.21 (d,  $J_{\text{CF}} = 8.7$  Hz);  $^{13}\text{C}\{\text{H}, ^{19}\text{F}\}$  NMR (100 MHz,  $\text{CDCl}_3$ )  $\delta$  149.19, 126.50, 125.19; HRMS (LDI-TOF MS) *m/z* calcd for  $\text{C}_{48}\text{H}_{16}\text{F}_{16} [\text{M}]^-$ : 896.1002, found: 896.0994.

## Synthesis of 2

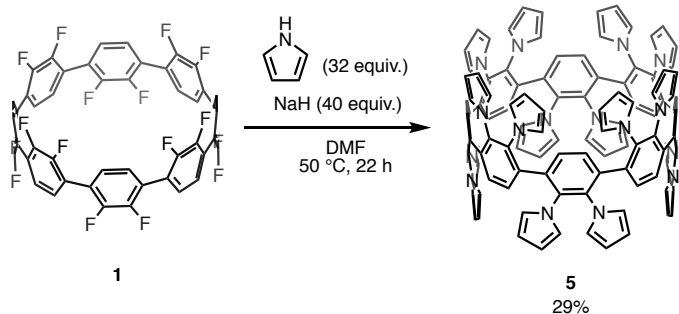


Gold complexes  $[\text{Au}_2\text{Cl}_2(\text{dcpm})]$  (dcpm: bis(dicyclohexylphosphino)methane) and  $[\text{Au}_2(\text{C}_6\text{F}_2\text{H}_2-\text{C}_6\text{F}_2\text{H}_2)(\text{dcpm})]_3$  used in this synthesis were prepared following the previous report.<sup>[S2]</sup> To a 50-mL two-neck round-bottom flask containing a magnetic stirring bar were added 2,2'-(2,2',3,3'-tetrafluoro-[1,1'-biphenyl]-4,4'-diyl)bis(4,4,5,5-tetramethyl-1,3,2-dioxaborolane) (99.1 mg, 207  $\mu\text{mol}$ ),  $[\text{Au}_2\text{Cl}_2(\text{dcpm})]$  (177 mg, 203  $\mu\text{mol}$ ), cesium carbonate (404 mg, 1.24 mmol), toluene (8.0 mL), ethanol (2.0 mL), and water (2.0 mL). The reaction mixture was stirred at 50 °C for 24 h. The reaction mixture was quenched by methanol (50 mL). The supernatant was removed and *in vacuo* to obtain  $[\text{Au}_2(\text{C}_6\text{F}_2\text{H}_2-\text{C}_6\text{F}_2\text{H}_2)(\text{dcpm})]_3$  as a white solid (156 mg), which was used without further purification.

To a 200-mL Schlenk tube containing a magnetic stirring bar were added  $[\text{Au}_2(\text{C}_6\text{F}_2\text{H}_2-\text{C}_6\text{F}_2\text{H}_2)(\text{dcpm})]_3$  (109 mg, 35.4  $\mu\text{mol}$ ), iodobenzene dichloride (37.5 mg, 136  $\mu\text{mol}$ ), and 1,2-dichloroethane (18 mL). The reaction mixture was stirred at 150 °C for 3 h. After cooling the reaction mixture to room temperature, the reaction mixture was roughly purified by short silica gel column chromatography (eluent: dichloromethane) and then evaporated *in vacuo*. The roughly purified material was further purified by PTLC (eluent: dichloromethane/hexane = 1:2) to afford 1 (1.2 mg, 3.8%) as a yellow solid.

$^1\text{H}$  NMR (600 MHz,  $\text{CDCl}_3$ )  $\delta$  7.40 (d,  $J_{\text{HF}} = 2.7$  Hz, 12H);  $^{19}\text{F}$  NMR (565 MHz,  $\text{CDCl}_3$ )  $\delta$  -140.68 (12F);  $^{13}\text{C}\{\text{H}\}$  NMR (150 MHz,  $\text{CDCl}_3$ )  $\delta$  149.23 (dd,  $J_{\text{CF}} = 257.9, 16.6$  Hz), 126.24 (s), 124.20 (d,  $J_{\text{CF}} = 7.2$  Hz);  $^{13}\text{C}\{\text{H}, \text{F}\}$  NMR (100 MHz,  $\text{CDCl}_3$ )  $\delta$  149.21, 126.23, 124.18; HRMS (LDI-TOF MS)  $m/z$  calcd for  $\text{C}_{36}\text{H}_{12}\text{F}_{12} [\text{M}]^+$ : 672.0742, found: 672.0747.

### Synthesis of 5



To a 20-mL Schlenk tube containing a magnetic stirring bar were added **1** (41.4 mg, 46.2  $\mu\text{mol}$ ), sodium hydride (60%, dispersion in paraffin liquid, 49.5 mg, 2.06 mmol), and DMF (3 mL). To the reaction mixture was added pyrrole (0.12 mL, 1.73 mmol). The reaction mixture was stirred at 50 °C for 22 h. After cooling the reaction mixture to room temperature, the reaction mixture was quenched by water. Then, the organic layer was extracted with ethyl acetate, dried over  $\text{Na}_2\text{SO}_4$ , and then evaporated *in vacuo*. The crude material was purified by PTLC  $\times$  2 times (eluent:  $\text{CHCl}_3/\text{hexane} = 2:1$  and then  $3:1$ ) to afford **5** (22.2 mg, 29%) as a pale-yellow solid.

$^1\text{H}$  NMR (600 MHz,  $\text{CDCl}_3$ ) see Fig. S24;  $^1\text{H}$  NMR (600 MHz,  $\text{DMSO}-d_6$ ) see Fig. S27;  $^{13}\text{C}\{\text{H}\}$  NMR (150 MHz,  $\text{CDCl}_3$ ) see Fig. S25;  $^{13}\text{C}\{\text{H}\}$  NMR (150 MHz,  $\text{DMSO}-d_6$ )  $\delta$  138.49, 134.92, 131.63, 124.65, 109.13; HRMS (LDI-TOF MS, cationizing agent: sodium trifluoroacetate ( $\text{NaTFA}$ ))  $m/z$  calcd for  $\text{C}_{112}\text{H}_{80}\text{N}_{16} [\text{M}+\text{Na}]^+$ : 1671.6644, found: 1671.6656.

### 3. Synthesis and purification



**Fig. S1.** Picture of silica gel column chromatography irradiated with a 365 nm UV lamp. Fraction with light blue fluorescence contains compound **1**.

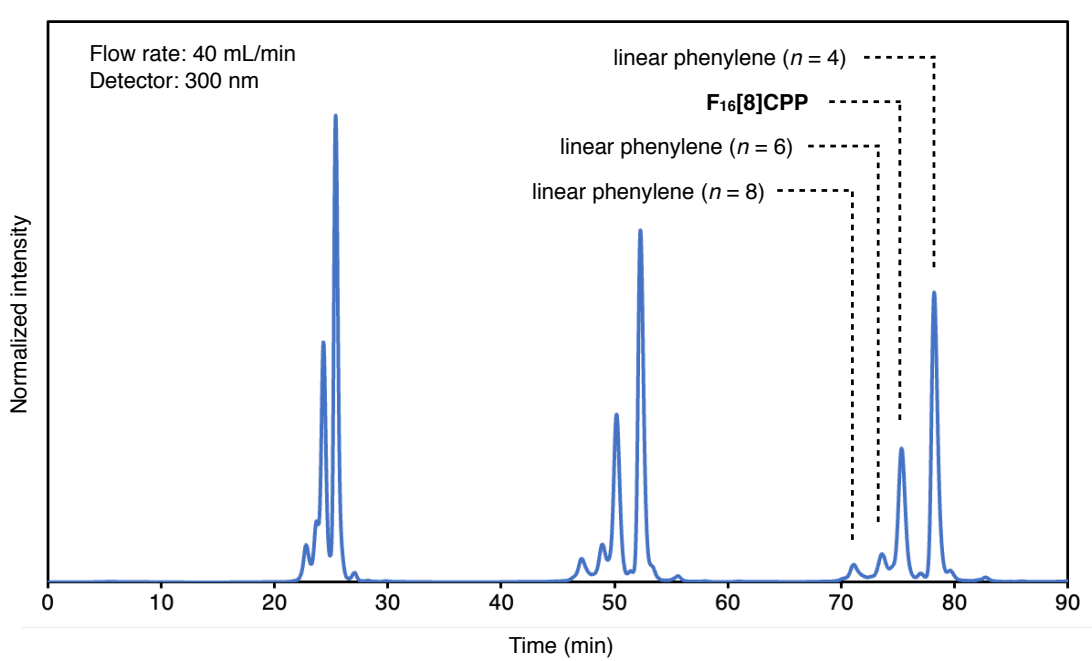


**Fig. S2.** The chromatogram of recycling preparative GPC of the crude mixture containing compound **1**.

#### 4. X-ray crystallography

Details of the crystal data and a summary of the intensity data collection parameters for **1**, **2**, and **5** are listed in Table S1. A suitable crystal was mounted with mineral oil on a MiTeGen MicroMounts and transferred to the goniometer of the kappa goniometer of a RIGAKU XtaLAB Synergy-S system with 1.2 kW MicroMax-007HF microfocus rotating anode (Graphite-monochromated Mo K $\alpha$  radiation ( $\lambda = 0.71073 \text{ \AA}$ )) and PILATUS200K hybrid photon-counting detector. Cell parameters were determined and refined, and raw frame data were integrated using CrysAlis<sup>Pro</sup> (Agilent Technologies, 2010). The structures were solved by direct methods with SHELXT<sup>[S4]</sup> and refined by full-matrix least-squares techniques against  $F^2$  (SHELXL-2018/3)<sup>[S5]</sup> by using Olex2 software package<sup>[S6]</sup>. The intensities were corrected for Lorentz and polarization effects. The non-hydrogen atoms were refined anisotropically. Hydrogen atoms were placed using AFIX instructions. CCDC 2057899, 2219047 and 2219046 contain the supplementary crystallographic data for this paper. These data can be obtained free of charge from The Cambridge Crystallographic Data Centre via [www.ccdc.cam.ac.uk/data\\_request/cif](http://www.ccdc.cam.ac.uk/data_request/cif).

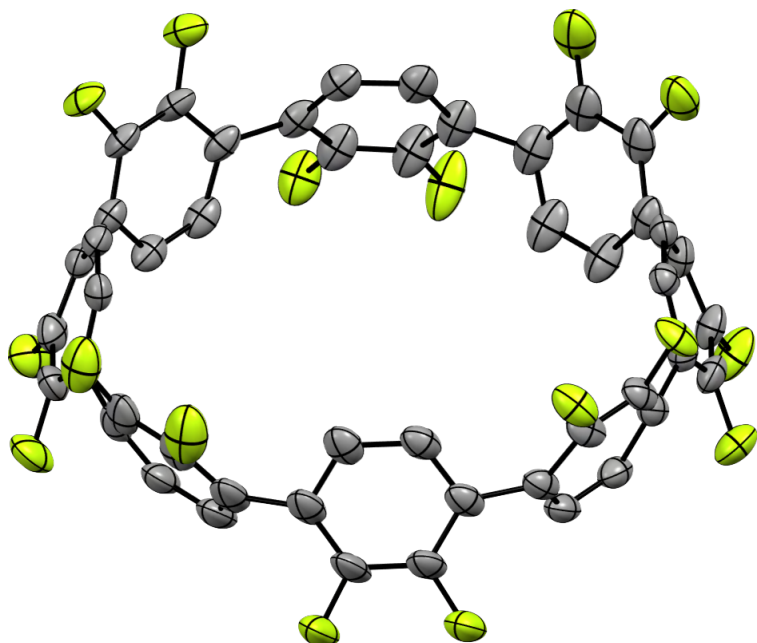


**Fig. S3.** ORTEP (Oak Ridge Thermal-Ellipsoid Plot) of **1** with 50% thermal probabilities. All hydrogen atoms and solvent molecules are omitted for clarity.

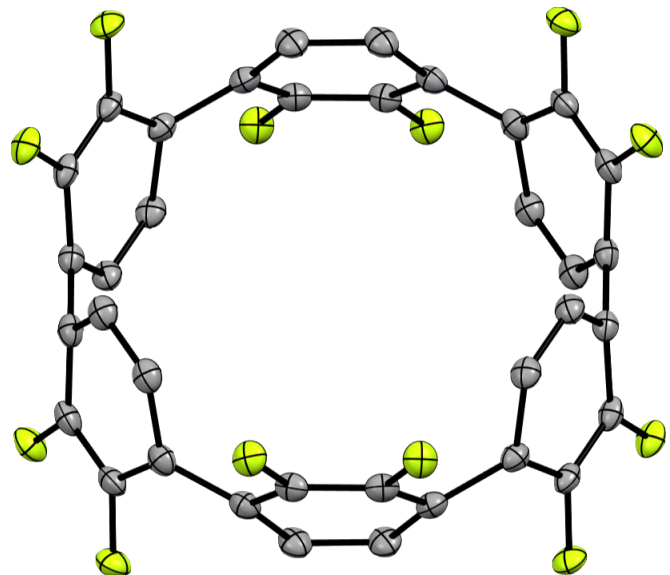


**Fig. S4.** ORTEP of **2** with 50% thermal probabilities. All hydrogen atoms and solvent molecules are omitted for clarity.

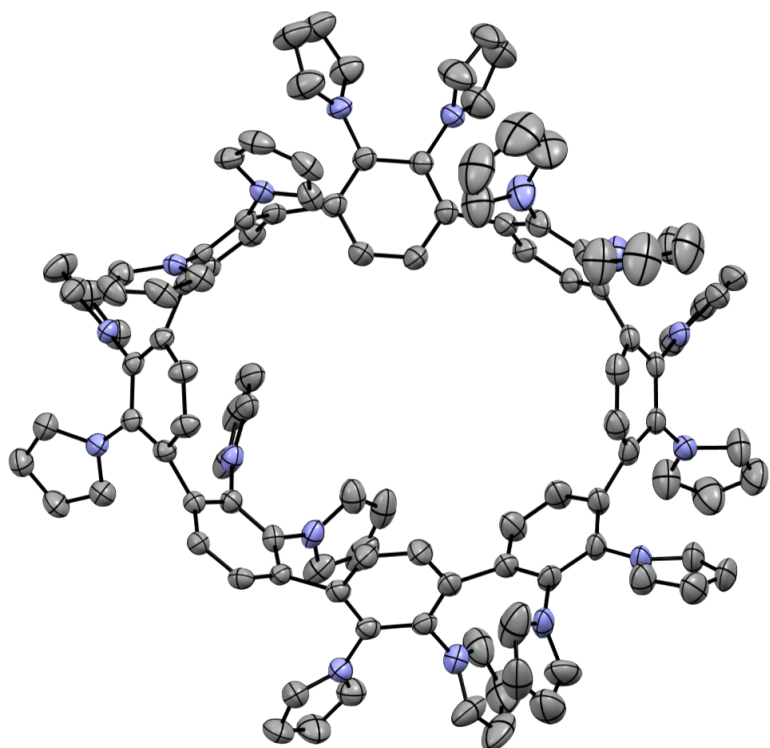


**Fig. S5.** ORTEP of **5** with 50% thermal probabilities. All hydrogen atoms and solvent molecules are omitted for clarity.

**Table S1.** Crystallographic data and structure refinement details of **1**, **2** and **5**

	<b>1</b>	<b>2</b>	<b>5</b>
CCDC No.	2057899	2219047	2219046
formula	C <sub>120</sub> H <sub>56</sub> F <sub>32</sub>	C <sub>44</sub> H <sub>28</sub> F <sub>12</sub> O <sub>2</sub>	C <sub>136</sub> H <sub>120</sub> N <sub>16</sub>
fw	2105.64	816.66	1978.47
T (K)	123(2)	123(2)	123(2)
λ (Å)	0.71073	0.71073	0.71073
cryst syst	monoclinic	triclinic	monoclinic
space group	<i>P</i> 2/c	<i>P</i> -1	<i>P</i> 2 <sub>1</sub> /c
<i>a</i> (Å)	19.8837(5)	9.9513(5)	19.1737(8)
<i>b</i> (Å)	18.2597(4)	10.4272(5)	23.2224(7)
<i>c</i> (Å)	27.4771(8)	10.5475(5)	25.1475(12)
α (deg)	90	112.645(5)	90
β (deg)	110.529(3)	100.614(4)	104.363(5)
γ (deg)	90	109.590(4)	90
<i>V</i> (Å <sup>3</sup> )	9342.6(4)	887.69(8)	10847.2(8)
<i>Z</i>	4	1	4
<i>D</i> <sub>calc</sub> (g·cm <sup>-3</sup> )	1.497	1.528	1.211
μ (mm <sup>-1</sup> )	0.131	0.136	0.072
F(000)	4256.0	416.0	4192.0
cryst size (mm <sup>3</sup> )	0.10 × 0.10 × 0.05	0.10 × 0.10 × 0.05	0.20 × 0.15 × 0.15
2θ range (deg)	3.124–54.188	4.486–59.642	3.344–55.95
reflns collected	58989	13568	64373
indep reflns/ <i>R</i> <sub>int</sub>	18190 / 0.0345	4167 / 0.0639	21583 / 0.0643
params	1703	353	1414
GOF on <i>F</i> <sup>2</sup>	1.035	1.061	1.027
<i>R</i> <sub>1</sub> , <i>wR</i> <sub>2</sub> [ <i>I</i> >2σ( <i>I</i> )]	0.0894, 0.2678	0.0816, 0.2272	0.1080, 0.2810
<i>R</i> <sub>1</sub> , <i>wR</i> <sub>2</sub> (all data)	0.1261, 0.3037	0.1062, 0.2456	0.1987, 0.3371

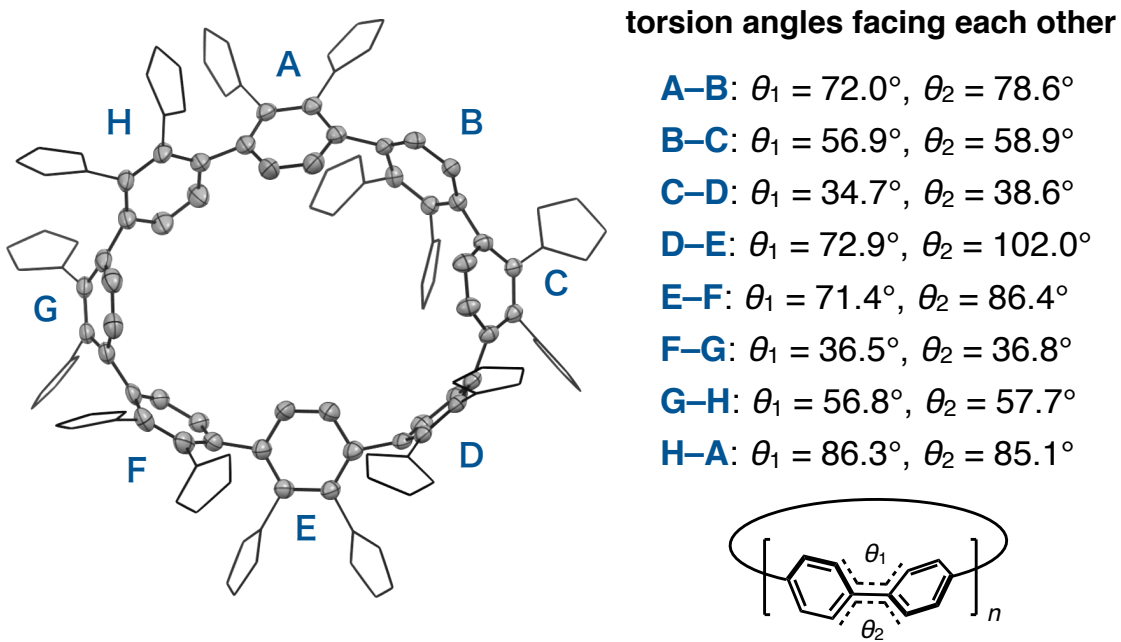


**Fig. S6.** Torsion angles facing each other. The main CPP structure is highly strained to the extent that one torsion angle exceeds 90 degrees.

**Table S2.** The average dihedral angles ( $\theta$ ) around the C–C single bonds of **1**, **2**, **5**, corresponding CPPs<sup>[S7,S8]</sup> and PFCPPs. Calculations were performed at the B3LYP/6-31+G(d) scrf CHCl<sub>3</sub> level in **1**, **2**, [6]CPP, [8]CPP, PF[6]CPP, and PF[8]CPP or the B3LYP/6-31G(d) level in **5** of theory. Dihedral angles obtained from X-ray crystallography are averaged.

	<b>2</b>	<b>1</b>	<b>5</b>	[6]CPP	[8]CPP	PF[6]CPP	PF[8]CPP
observed torsion angles	27.4°	36.8°	64.5°	28.1°	24.3°	—	—
calculated torsion angles	30.9°	36.6°	65.3°	27.0°	30.7°	47.3°	52.4°

**1**, **2**, [6]CPP, [8]CPP, PF[6]CPP, and PF[8]CPP: calculation at B3LYP/6-31+G(d) scrf CHCl<sub>3</sub>

**5**: calculation at B3LYP/6-31G(d), S<sub>8</sub> symmetry structure

[6]CPP crystal structure: ccdc number 871414

[8]CPP crystal structure: ccdc number 1841065

## 5. Photophysical measurements

UV–Vis absorption spectra were recorded on a Shimadzu UV-3600 spectrometer with a resolution of 0.5 nm. Dilute solutions in spectral grade dichloromethane in a 1 cm square quartz cell were used for measurements. Fluorescence spectra were recorded with a Shimadzu RF6000 spectrofluorometer using a 3 nm bandwidth in emission. Absolute quantum yields ( $\Phi$ ) were determined with a Hamamatsu Photonics C11347-01 Absolute quantum yield spectrometer (Quantaurus-QY) equipped with an integrating sphere.

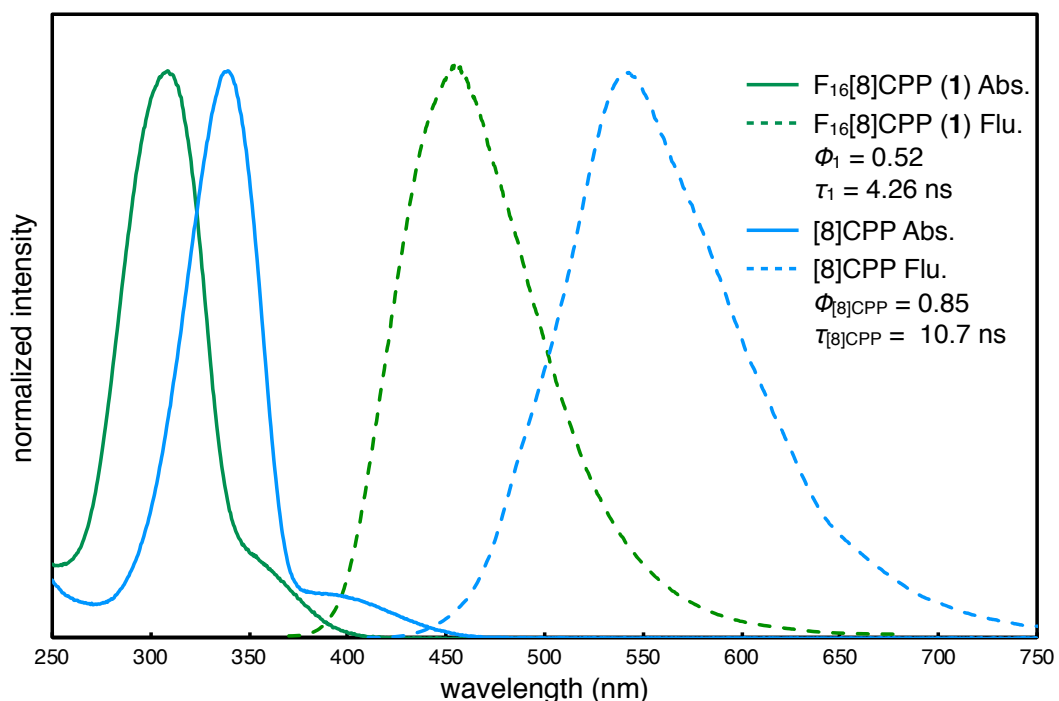


**Fig. S7.** UV–Vis absorption, fluorescence spectra, quantum yields, and life time of the diluted dichloromethane solution of **1** and [8]cycloparaphenylenne (CPP).

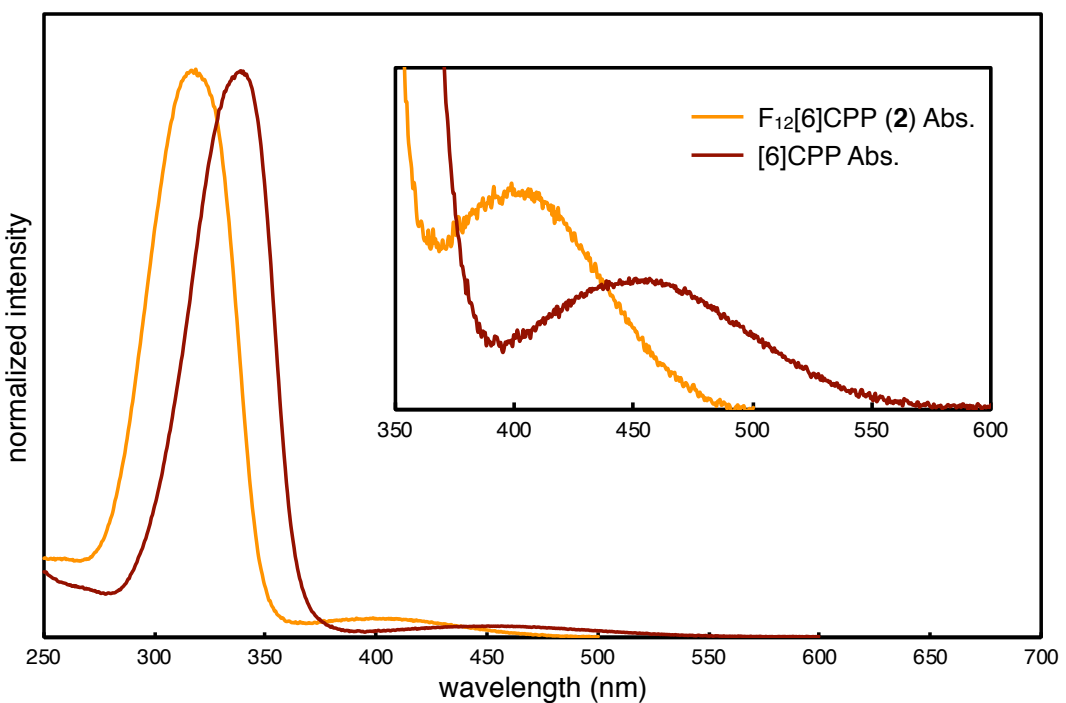


**Fig. S8.** UV–Vis absorption spectra of the diluted dichloromethane solution of **2** and [6]CPP.

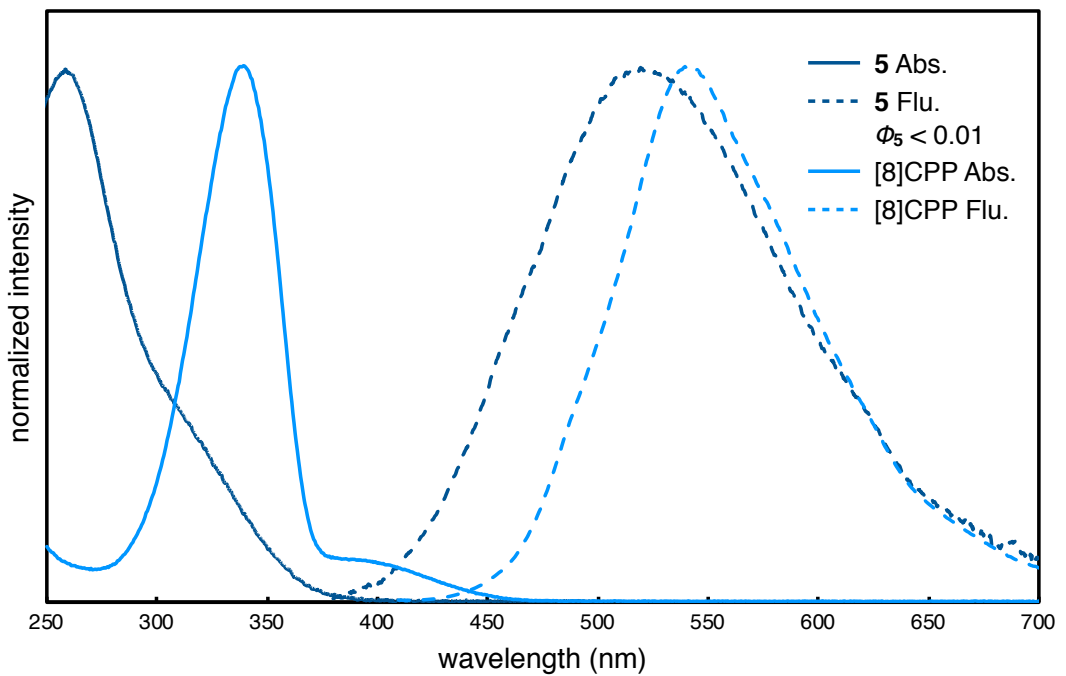


**Fig. S9.** UV–Vis absorption and fluorescence spectra of the diluted dichloromethane solution of **5** and [8]CPP.

## 6. Electrochemical measurements

Cyclic voltammetry (CV) was performed on a BAS ALS620A electrochemical analyzer. The CV cell consisted of a Pt working electrode, a Pt wire counter electrode, and a titanium reference electrode. The measurements were carried out under an argon atmosphere using a acetonitrile solution of a sample with a concentration of 1.0 mM and 0.1 M tetrabutylammonium hexafluorophosphate (*n*-Bu<sub>4</sub>NPF<sub>6</sub>) as a supporting electrolyte. The redox potentials were calibrated with ferrocene as an internal standard.

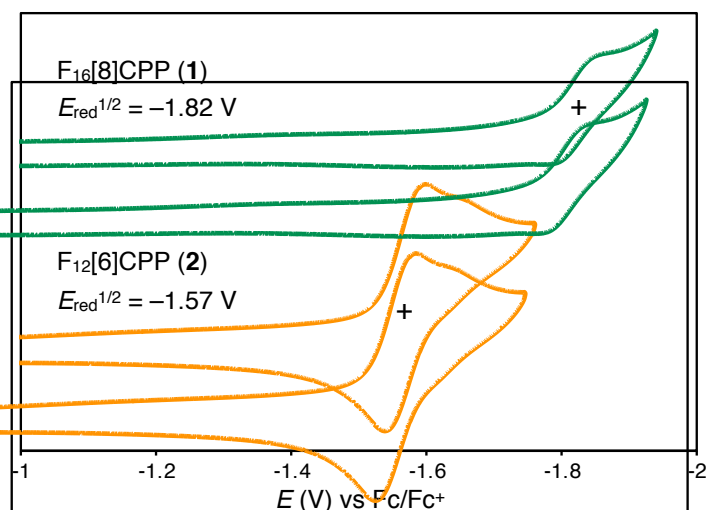


**Fig. S10.** Cyclic voltammograms of **1** and **2** in acetonitrile, measured with  $n\text{-Bu}_4\text{NPF}_6$  (0.1 M) as a supporting electrolyte at a scan rate of 100 mV s<sup>-1</sup>.

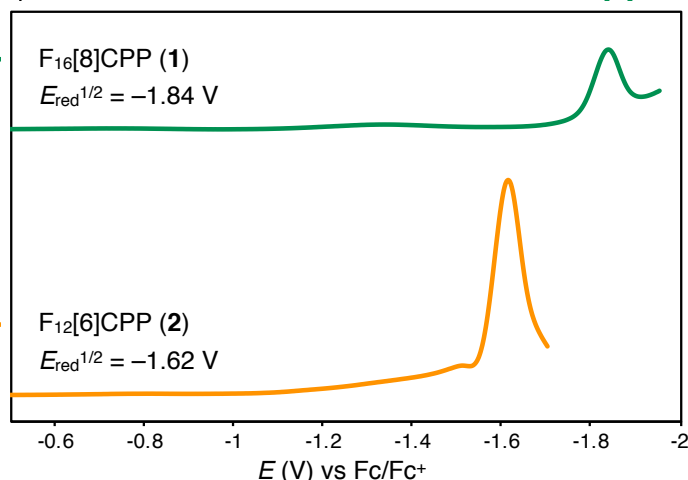


**Fig. S11.** Differential pulse voltammograms of **1** and **2** in acetonitrile, measured with  $n\text{-Bu}_4\text{NPF}_6$  (0.1 M) as a supporting electrolyte at a scan rate of 8.0 mV s<sup>-1</sup>.

## 7. Computational studies

The Gaussian 16 program<sup>[S9]</sup> running on a NEC LX 110Rh system was used for optimization (B3LYP/6-31+G(d)<sup>[S10,S11]</sup> with scrf CHCl<sub>3</sub> condition. In addition, compound **5** was optimized at B3LYP/6-31G(d) condition. Only highly symmetric structure (*S*<sub>8</sub> symmetry) in optimization gave the most stable structure without imaginary vibrations. Structures were optimized without any symmetry assumptions. Structures were optimized without any symmetry assumptions. Zero-point energy, enthalpy, and Gibbs free energy at 298.15 K and 1 atm were estimated from the gas-phase studies. Harmonic vibration frequency calculation at the same level was performed to verify all stationary points as local minima (with no imaginary frequency). NCI plot<sup>[S12,S13]</sup> was calculated by a NCIPILOT 4.0 program using optimized structures of hexadecapyrrolyl[8]CPP.

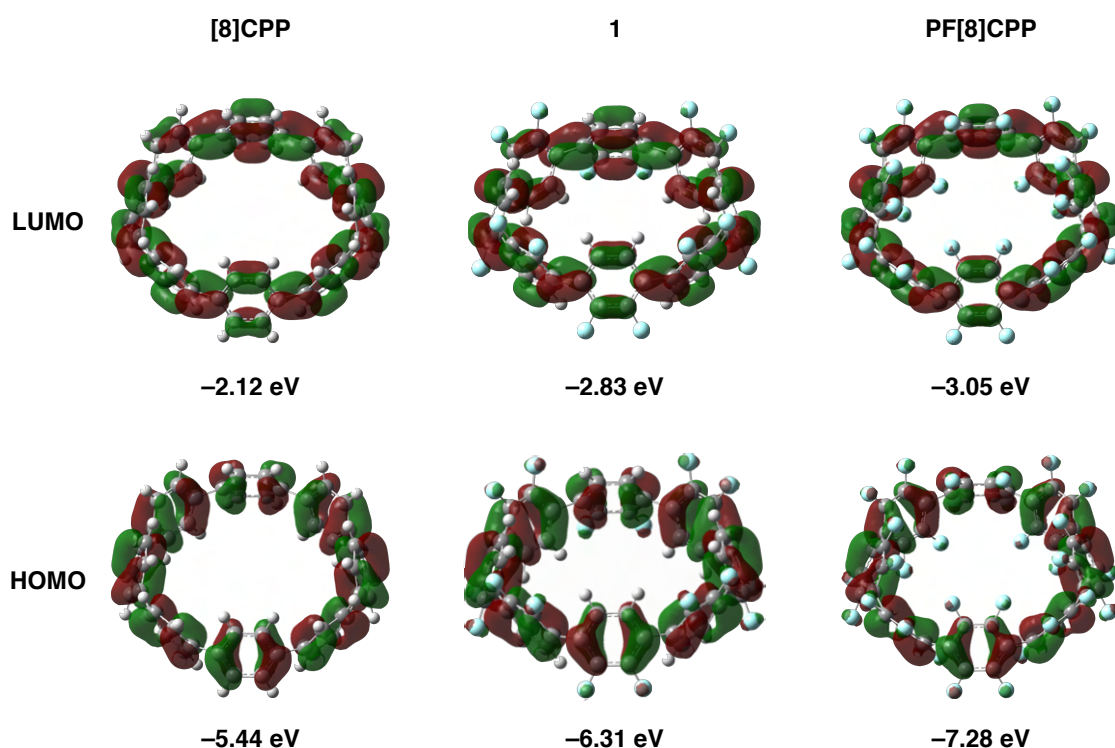


**Fig. S12.** Frontier molecular orbitals of [8]CPP, **1**, and PF[8]CPP. Isovalue: 0.02.

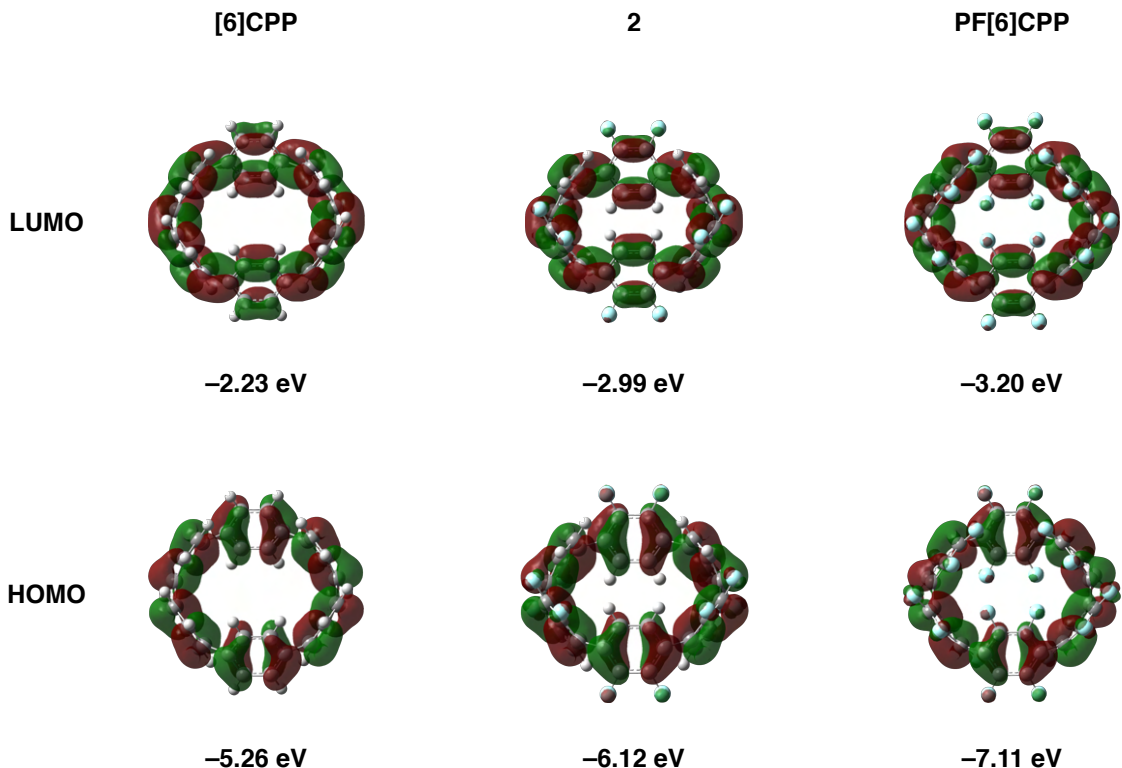


**Fig. S13.** Frontier molecular orbitals of [6]CPP, **2**, and PF[6]CPP. Isovalue: 0.02.

**Table S3.** Uncorrected and thermal-corrected (298 K) energies of stationary points (Hartree).<sup>a</sup>

	<i>E</i>	<i>E + ZPE</i>	<i>H</i>	<i>G</i>
<b>1</b>	-3436.191087	-3435.679063	-3435.628006	-3435.762570
<b>2</b>	-2577.078812	-2576.695306	-2576.657652	-2576.761347
<b>[8]CPP</b>	-1848.411236	-1847.766362	-1847.730548	-1847.830611
<b>[6]CPP</b>	-1386.242609	-1385.760042	-1385.733725	-1385.813207
<b>PF[8]CPP</b>	-5023.903635	-5023.524290	-5023.458548	-5023.622576
<b>PF[6]CPP</b>	-3767.853089	-3767.569157	-3767.520724	-3767.645936

a) *E*: electronic energy; *ZPE*: zero-point energy; *H* ( $= E + ZPE + E_{\text{vib}} + E_{\text{rot}} + E_{\text{trans}} + RT$ ): sum of electronic and thermal enthalpies; *G* ( $= H - TS$ ): sum of electronic and thermal free energies.

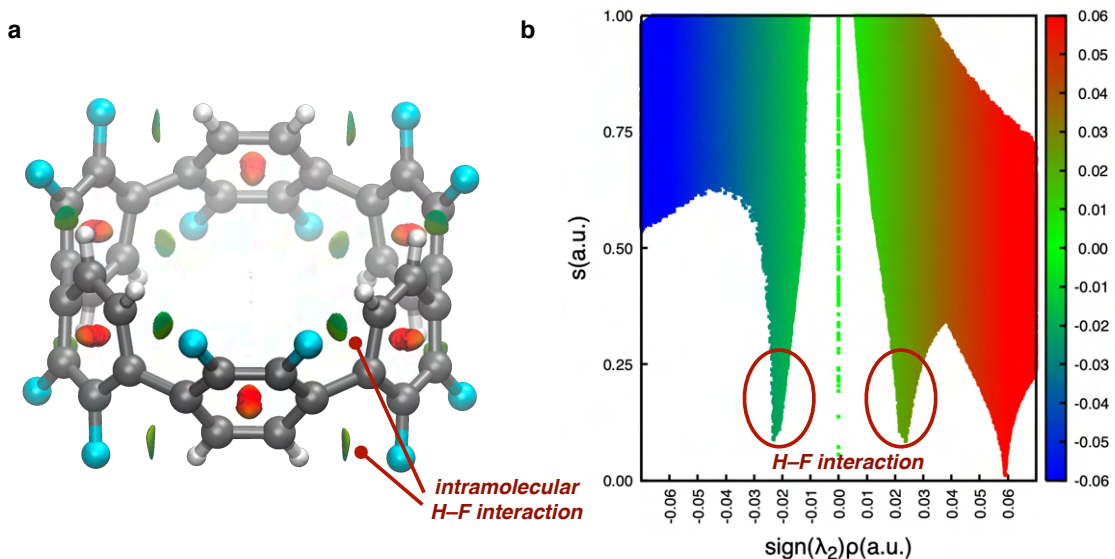


**Fig. S14.** (a) NCI plot of **2** visualizing intramolecular interactions by using X-ray structure. An isosurface value of 0.25 a.u. is applied to the structure. (b) The color scale ranges from  $-0.07$  (blue) to  $0.07$  (red) a.u. Large, negative values of  $\text{sign}(\lambda_2)\rho$  indicate an attractive interaction. Large, positive values reflect strong non-bonded overlapping, which generally results from steric repulsion. Values near zero correspond to the magnitude of the van der Waals interaction.

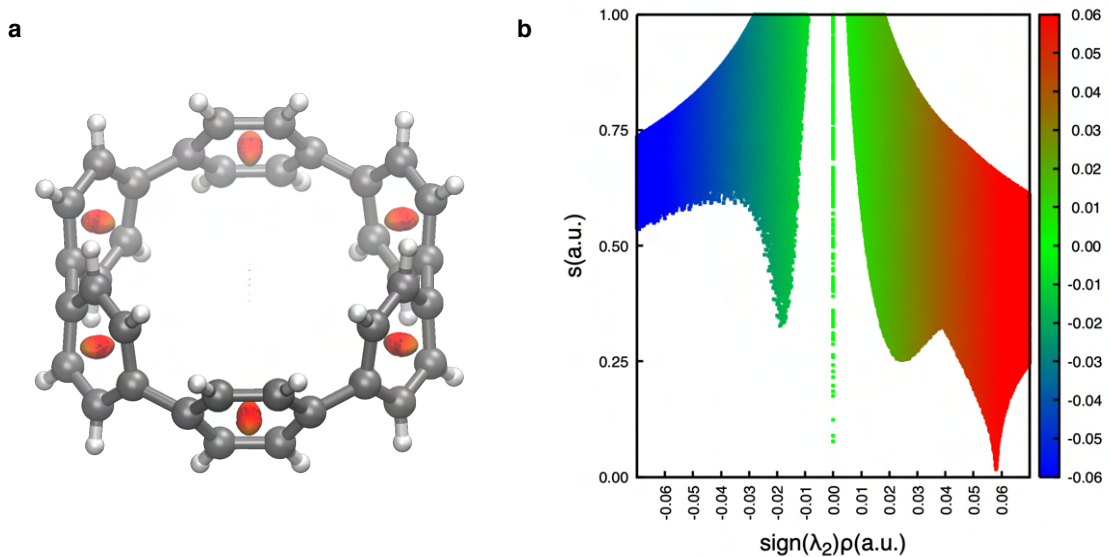


**Fig. S15.** (a) NCI plot of [6]CPP visualizing intramolecular interactions by using X-ray structure.<sup>[S7]</sup> An isosurface value of 0.25 a.u. is applied to the structure. (b) The color scale ranges from  $-0.07$  (blue) to  $0.07$  (red) a.u. Large, negative values of  $\text{sign}(\lambda_2)\rho$  indicate an attractive interaction. Large, positive values reflect strong non-bonded overlapping, which generally results from steric repulsion. Values near zero correspond to the magnitude of the van der Waals interaction.

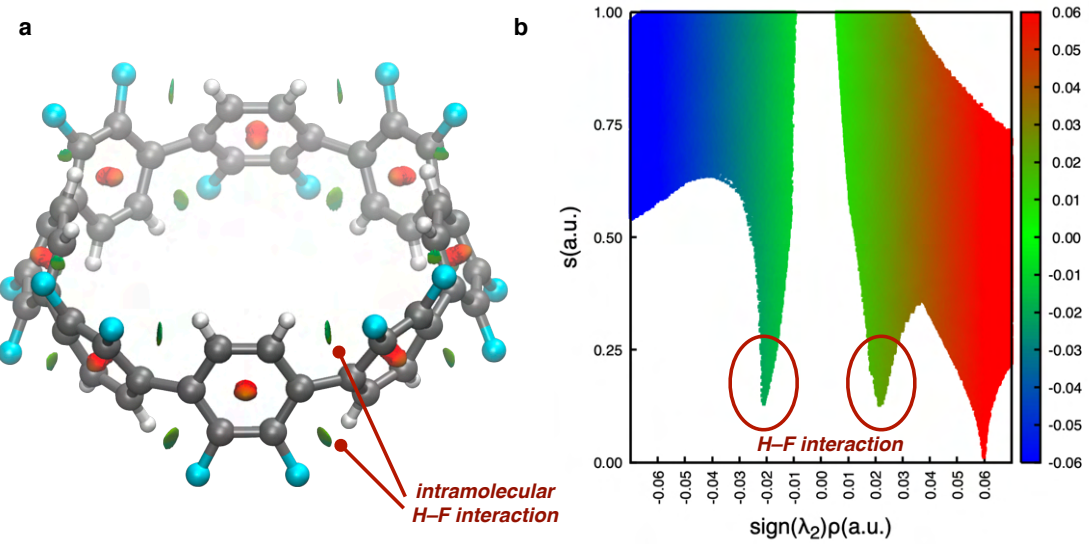


**Fig. S16.** (a) NCI plot of **1** visualizing intramolecular interactions by using X-ray structure. An isosurface value of 0.25 a.u. is applied to the structure. (b) The color scale ranges from  $-0.07$  (blue) to  $0.07$  (red) a.u. Large, negative values of  $\text{sign}(\lambda_2)\rho$  indicate an attractive interaction. Large, positive values reflect strong non-bonded overlapping, which generally results from steric repulsion. Values near zero correspond to the magnitude of the van der Waals interaction.

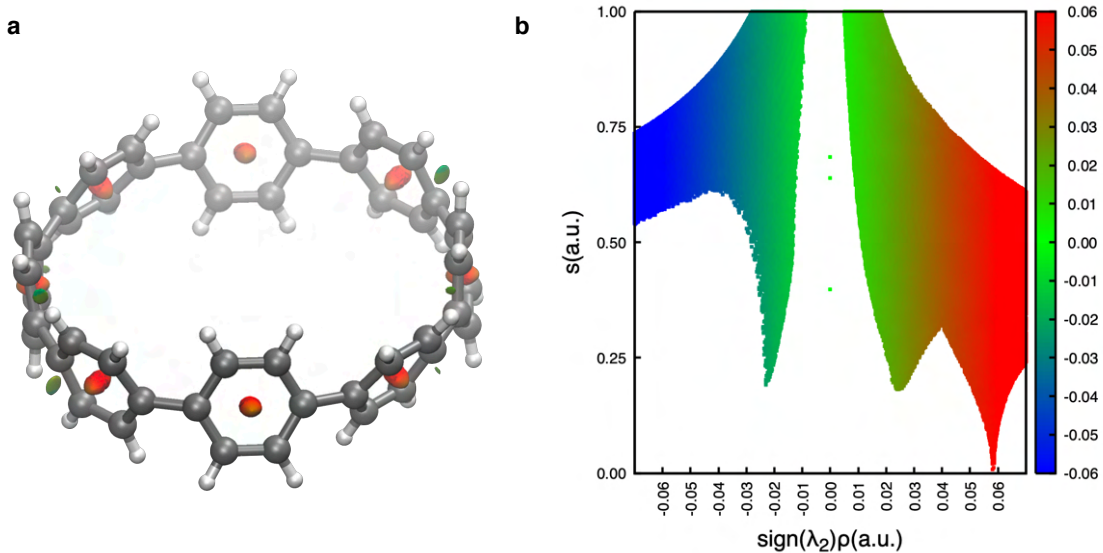


**Fig. S17.** (a) NCI plot of [8]CPP visualizing intramolecular interactions by using X-ray structure. [S8] An isosurface value of 0.25 a.u. is applied to the structure. (b) The color scale ranges from  $-0.07$  (blue) to  $0.07$  (red) a.u. Large, negative values of  $\text{sign}(\lambda_2)\rho$  indicate an attractive interaction. Large, positive values reflect strong non-bonded overlapping, which generally results from steric repulsion. Values near zero correspond to the magnitude of the van der Waals interaction.

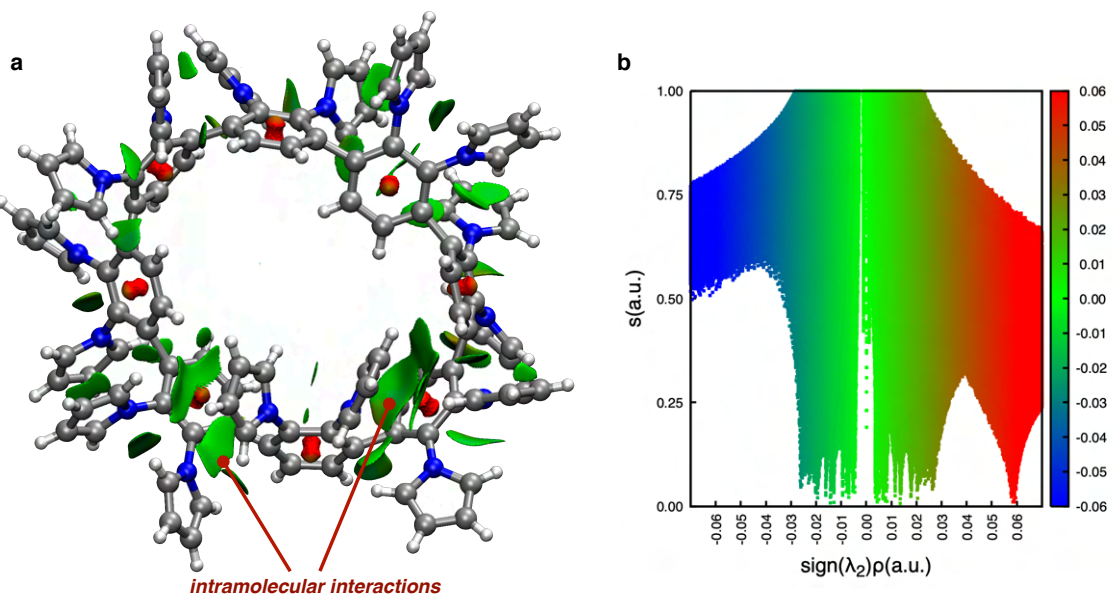


**Fig. S18.** (a) NCI plot of **5** visualizing intramolecular interactions by using X-ray structure. An isosurface value of 0.3 a.u. is applied to the structure. (b) The color scale ranges from  $-0.07$  (blue) to  $0.07$  (red) a.u. Large, negative values of  $\text{sign}(\lambda_2)\rho$  indicate an attractive interaction. Large, positive values reflect strong non-bonded overlapping, which generally results from steric repulsion. Values near zero correspond to the magnitude of the van der Waals interaction.

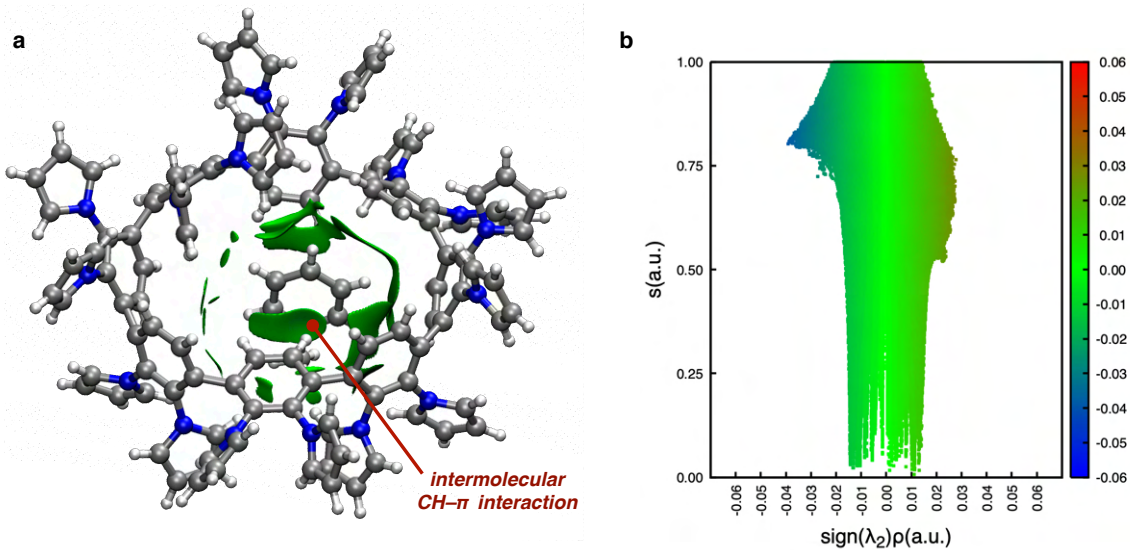


**Fig. S19.** (a) NCI plot of visualizing intermolecular interactions between **5** and toluene. An isosurface value of 0.3 a.u. is applied to the structure. (b) The color scale ranges from  $-0.07$  (blue) to  $0.07$  (red) a.u. Large, negative values of  $\text{sign}(\lambda_2)\rho$  indicate an attractive interaction. Large, positive values reflect strong non-bonded overlapping, which generally results from steric repulsion. Values near zero correspond to the magnitude of the van der Waals interaction.









## 8. NMR spectra of 1, 2, and 4

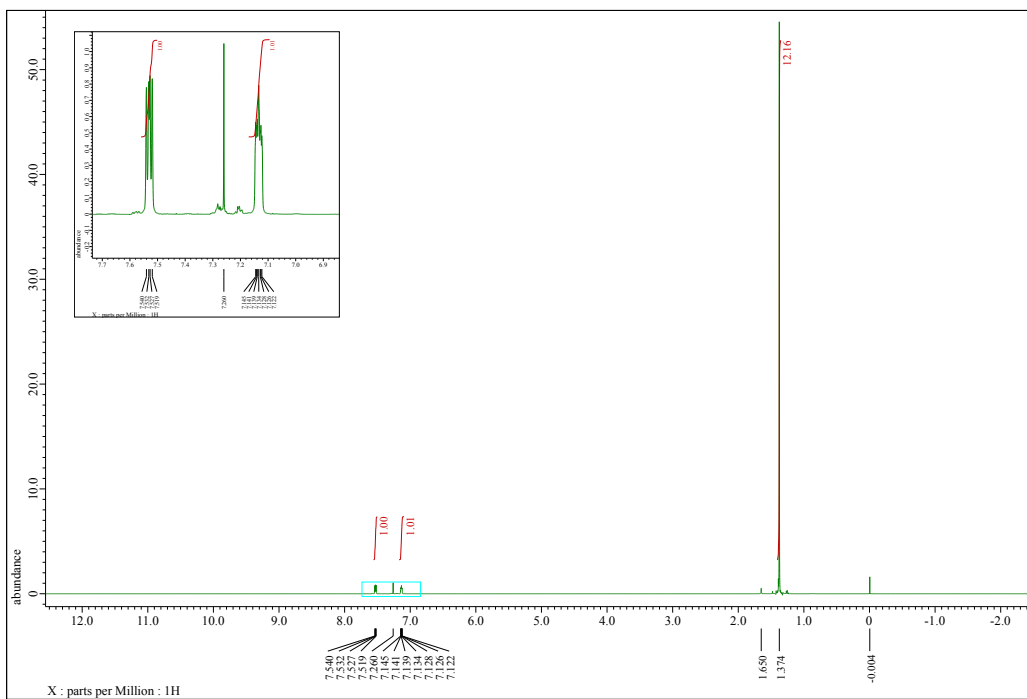


**Fig. S20.**  $^1\text{H}$  NMR spectrum of **4** (600 MHz,  $\text{CDCl}_3$ ). Reference:  $\text{CHCl}_3$  (7.26 ppm)

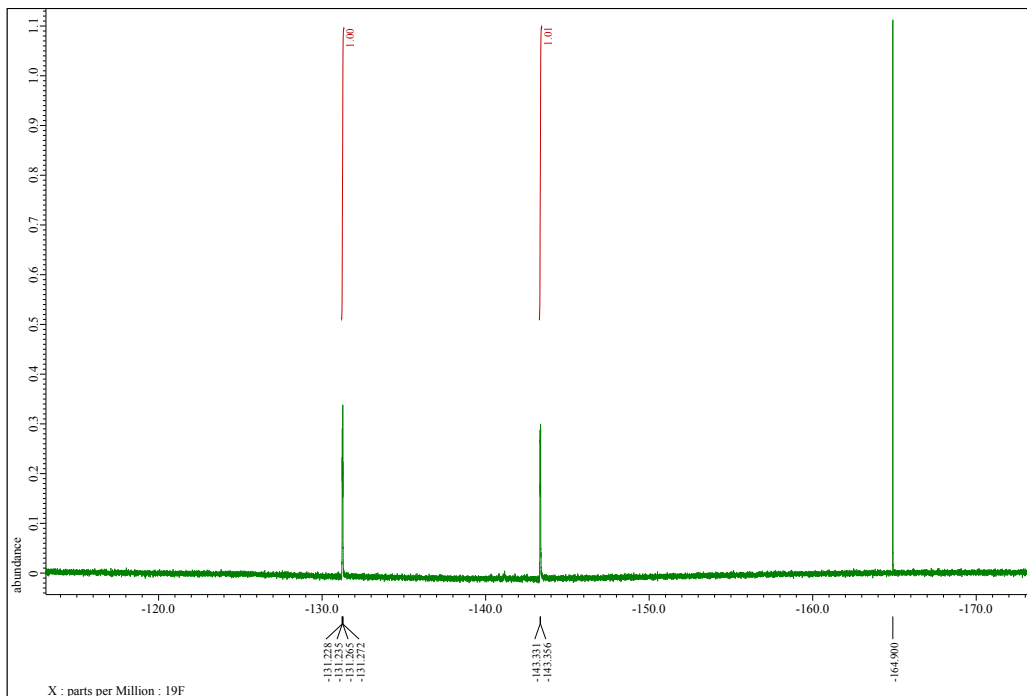


**Fig. S21.**  $^{19}\text{F}$  NMR spectrum of **4** (565 MHz,  $\text{CDCl}_3$ ). Reference:  $\text{C}_6\text{F}_6$  ( $-164.9$  ppm)

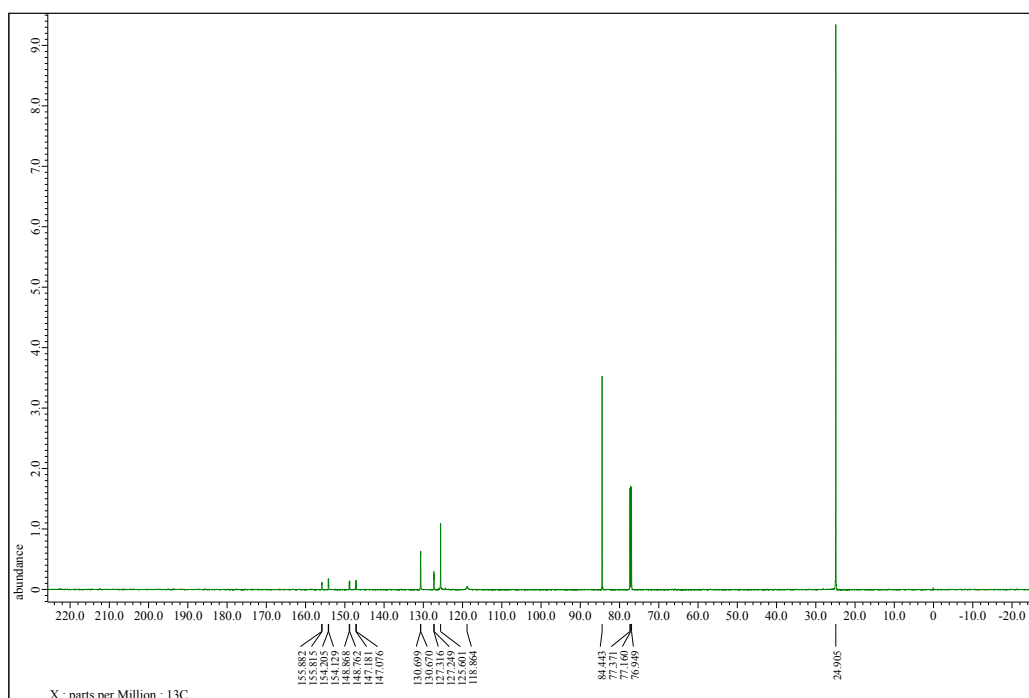


**Fig. S22.**  $^{13}\text{C}\{^1\text{H}\}$  NMR spectrum of **4** (150 MHz,  $\text{CDCl}_3$ ). Reference:  $\text{CDCl}_3$  (77.16 ppm)

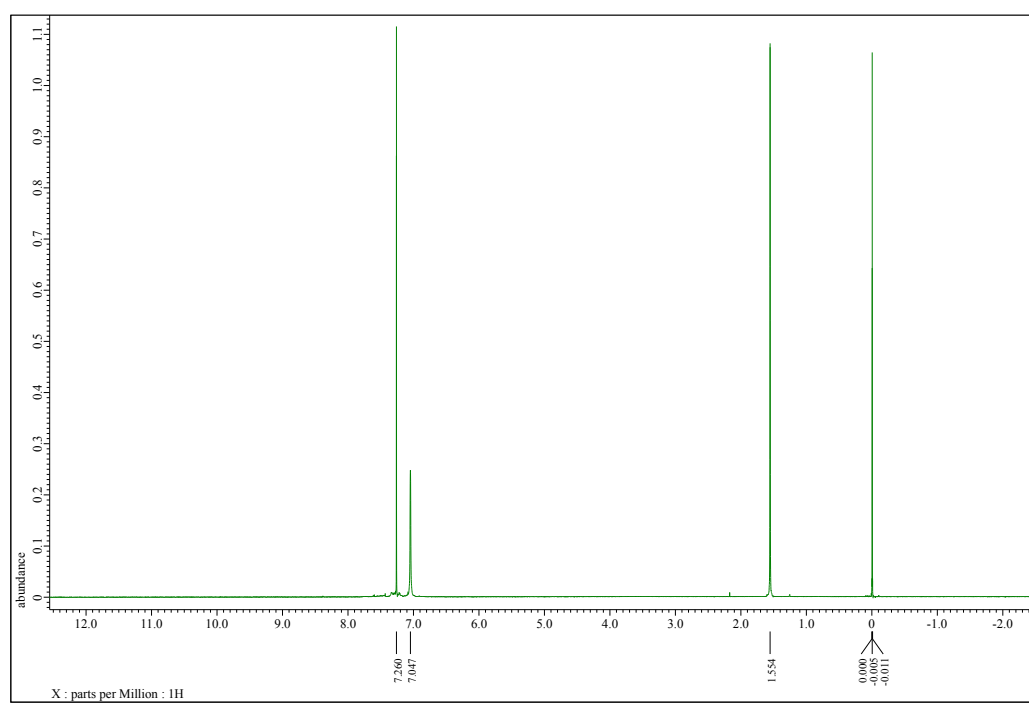


**Fig. S23.**  $^1\text{H}$  NMR spectrum of **1** (600 MHz,  $\text{CDCl}_3$ ). Reference:  $\text{CHCl}_3$  (7.26 ppm)

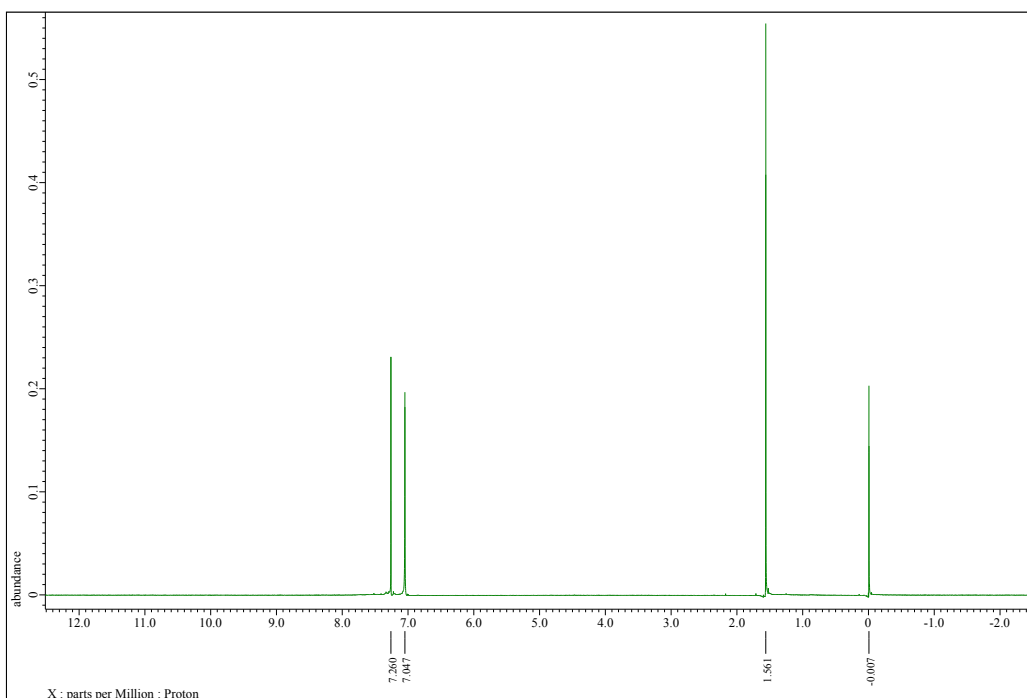


**Fig. S24.**  $^1\text{H}\{^{19}\text{F}\}$  NMR spectrum of **1** (400 MHz,  $\text{CDCl}_3$ ). Reference:  $\text{CHCl}_3$  (7.26 ppm)

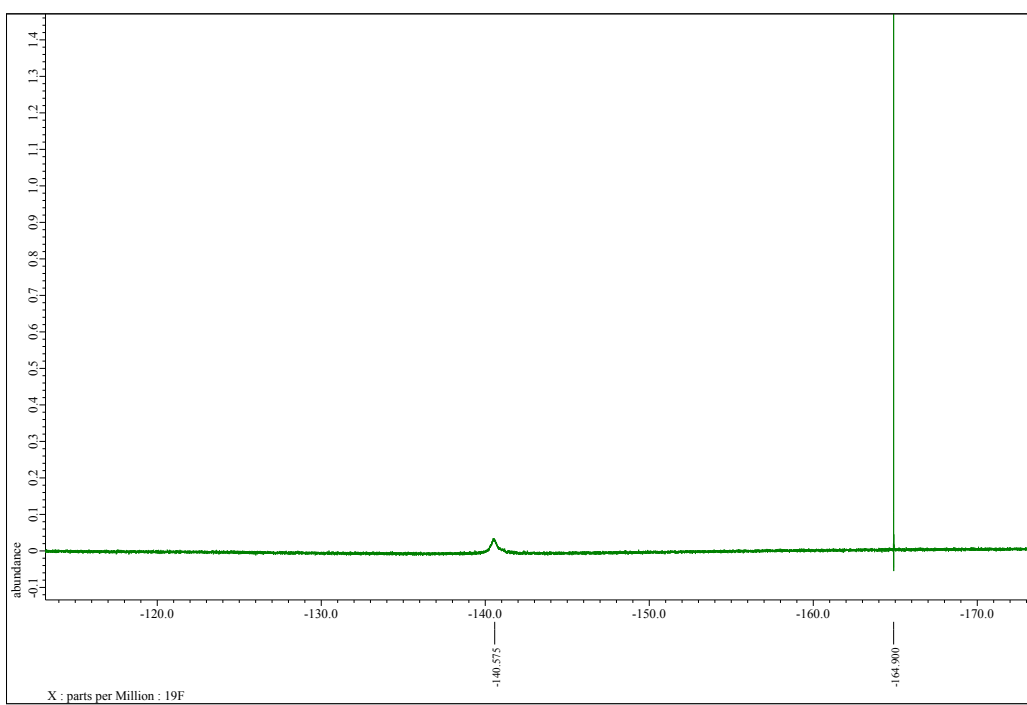


**Fig. S25.**  $^{19}\text{F}$  NMR spectrum of **1** (565 MHz,  $\text{CDCl}_3$ ). Reference:  $\text{C}_6\text{F}_6$  (-164.9 ppm)

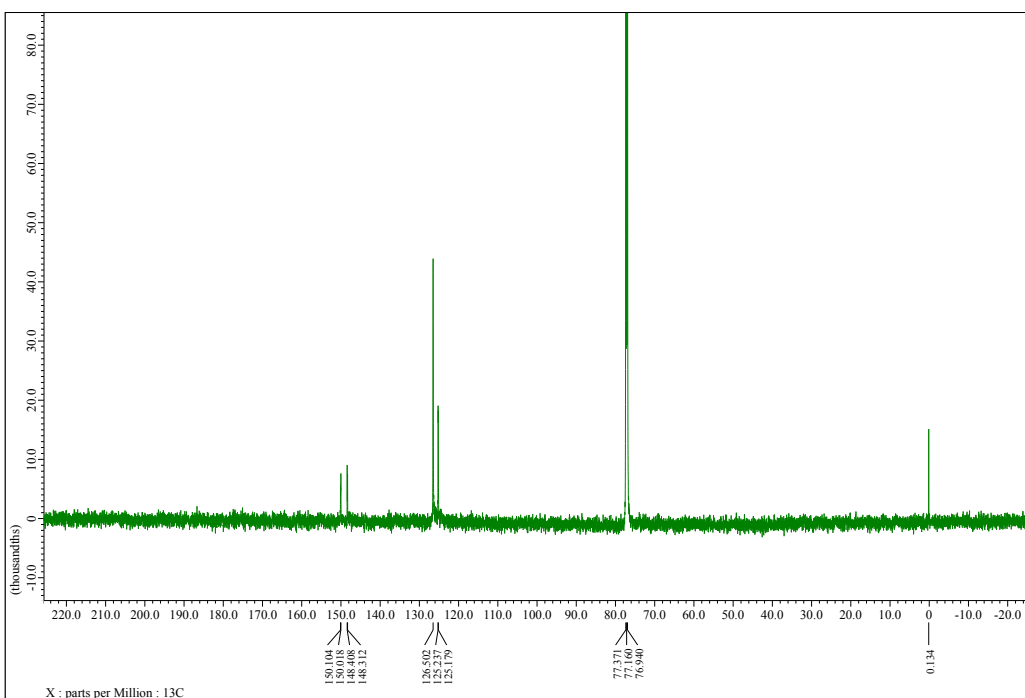


**Fig. S26.**  $^{13}\text{C}\{^1\text{H}\}$  NMR spectrum of **1** (150 MHz,  $\text{CDCl}_3$ ). Reference:  $\text{CDCl}_3$  (77.16 ppm)

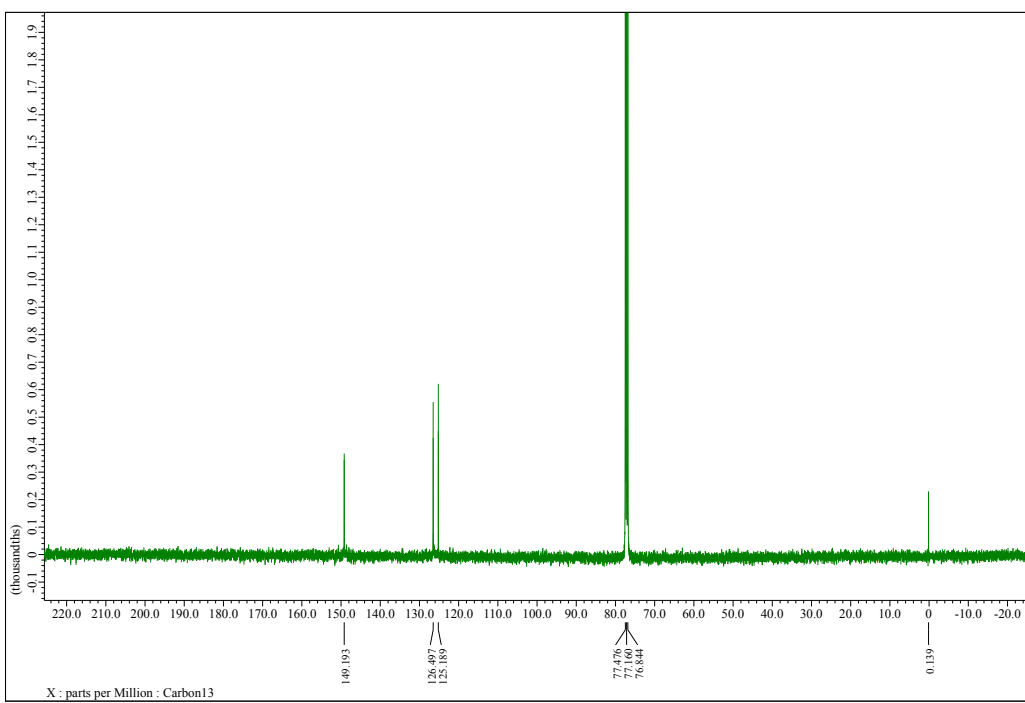


**Fig. S27.**  $^{13}\text{C}\{^1\text{H}, ^{19}\text{F}\}$  NMR spectrum of **1** (100 MHz,  $\text{CDCl}_3$ ). Reference:  $\text{CDCl}_3$  (77.16 ppm)

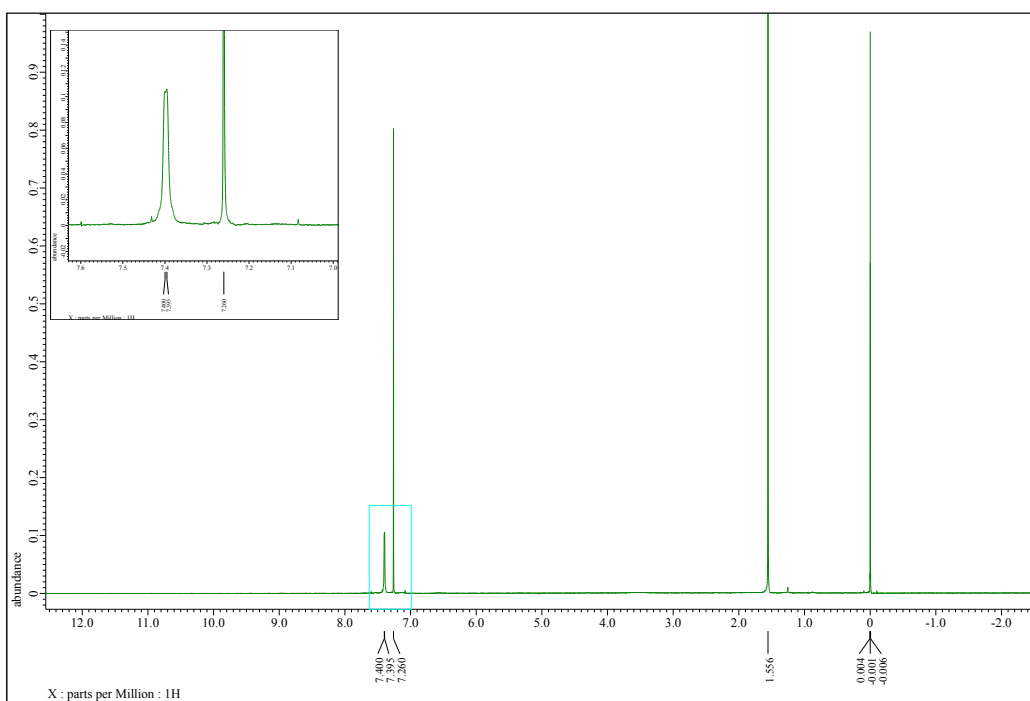


**Fig. S28.**  $^1\text{H}$  NMR spectrum of **2** (600 MHz,  $\text{CDCl}_3$ ). Reference:  $\text{CHCl}_3$  (7.26 ppm)

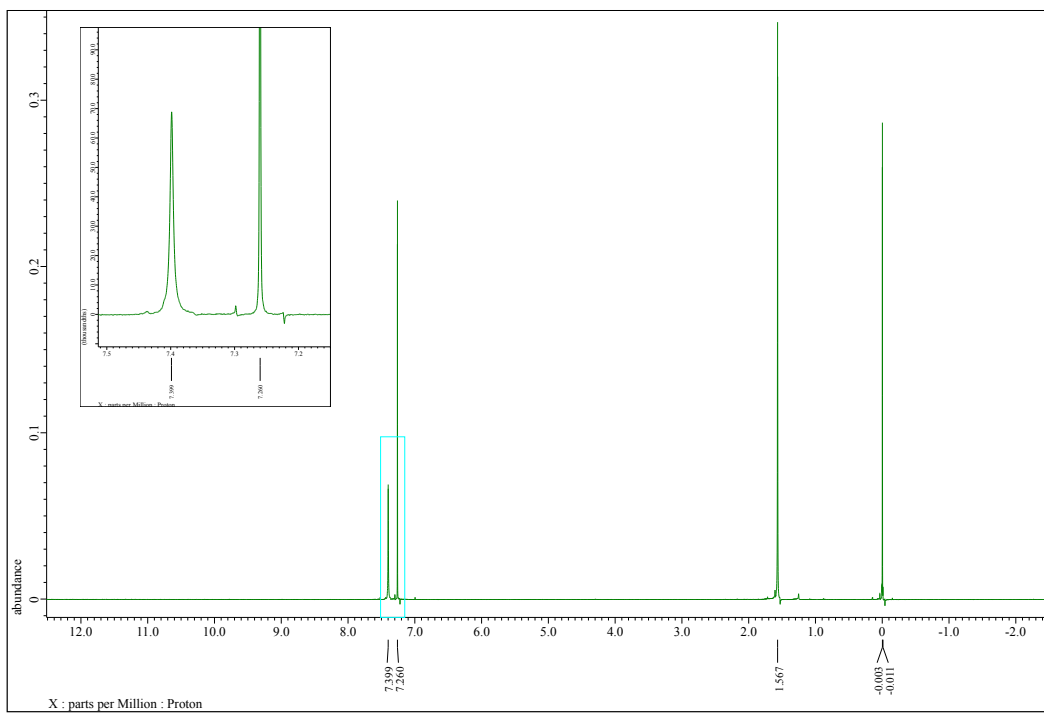


**Fig. S29.**  $^1\text{H}\{\text{F}^{19}\}$  NMR spectrum of **2** (400 MHz,  $\text{CDCl}_3$ ). Reference:  $\text{CHCl}_3$  (7.26 ppm)

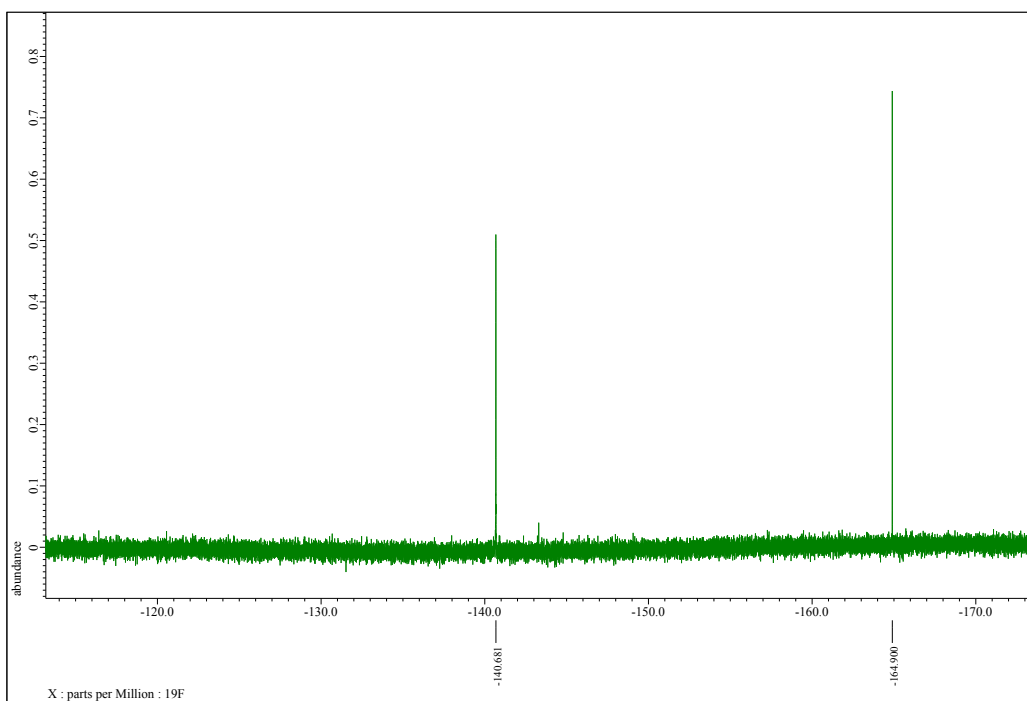


**Fig. S30.**  $^{19}\text{F}$  NMR spectrum of **2** (565 MHz,  $\text{CDCl}_3$ ). Reference:  $\text{C}_6\text{F}_6$  ( $-164.9$  ppm)

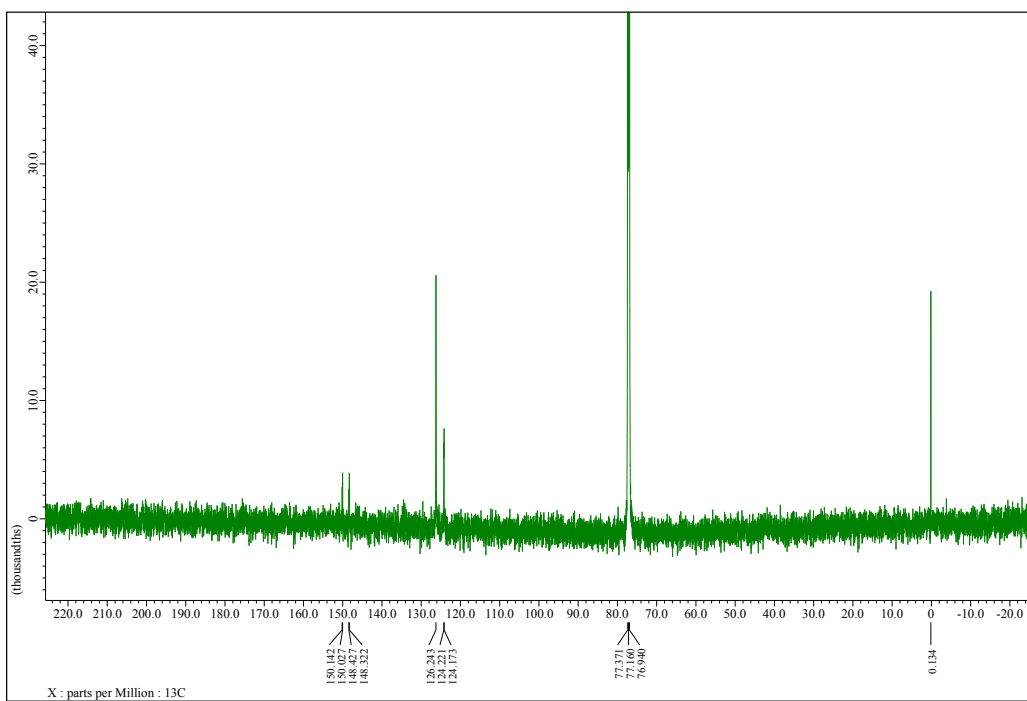


**Fig. S31.**  $^{13}\text{C}\{^1\text{H}\}$  NMR spectrum of **2** (150 MHz,  $\text{CDCl}_3$ ). Reference:  $\text{CDCl}_3$  (77.16 ppm)

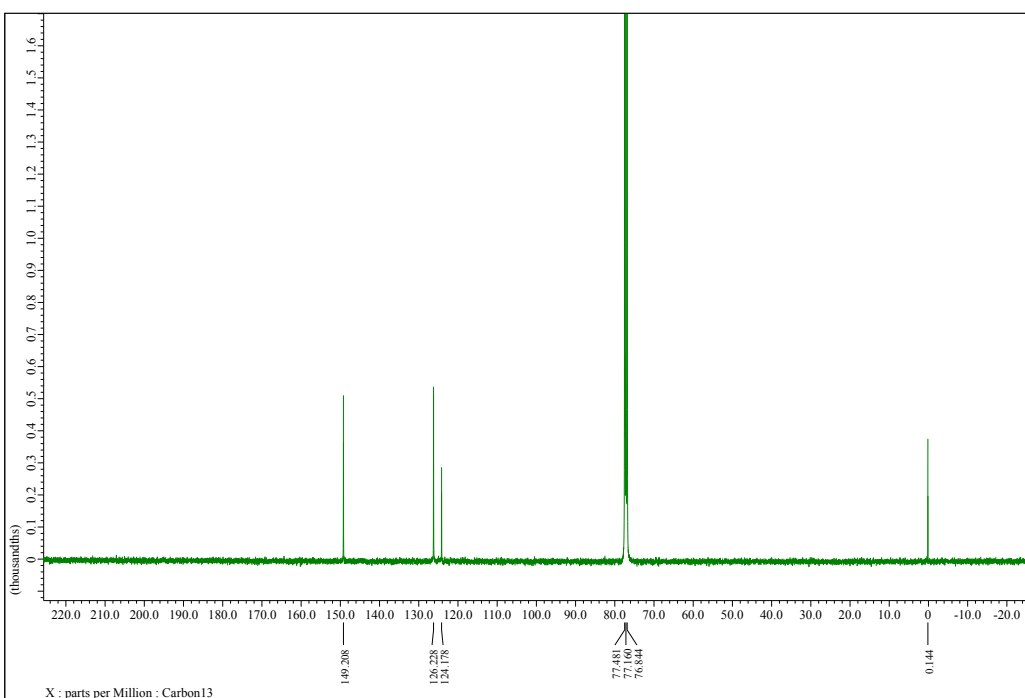


**Fig. S32.**  $^{13}\text{C}$  { $^1\text{H}, ^{19}\text{F}$ } NMR spectrum of **2** (100 MHz,  $\text{CDCl}_3$ ). Reference:  $\text{CDCl}_3$  (77.16 ppm)

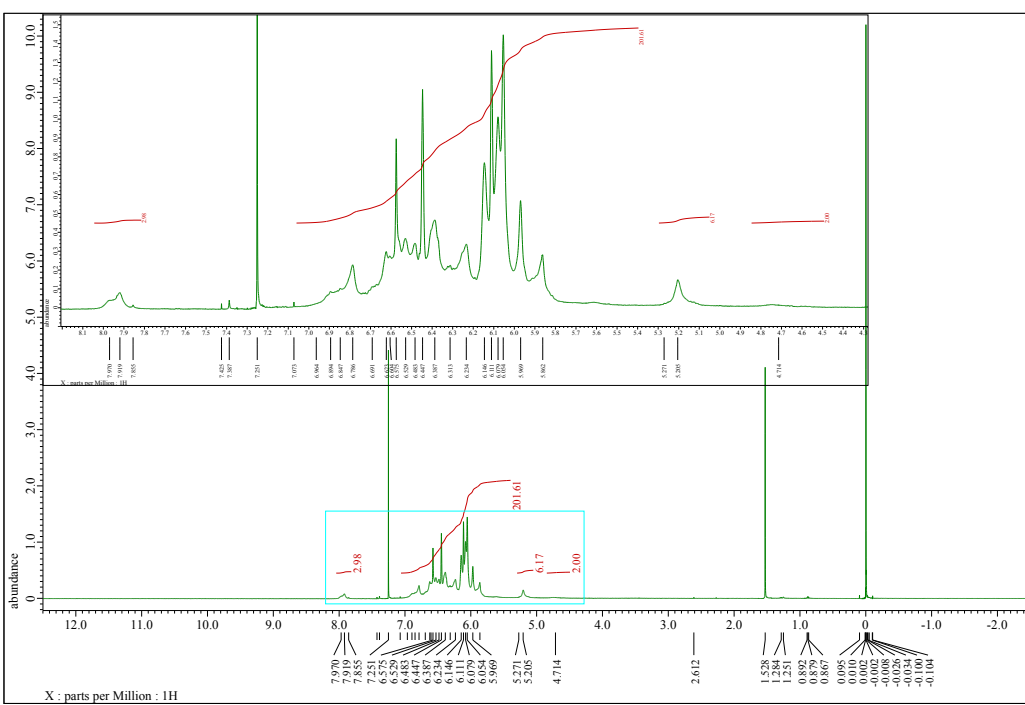


**Fig. S33.**  $^1\text{H}$  NMR spectrum of **5** (600 MHz,  $\text{CDCl}_3$ ). Reference:  $\text{CHCl}_3$  (7.26 ppm)

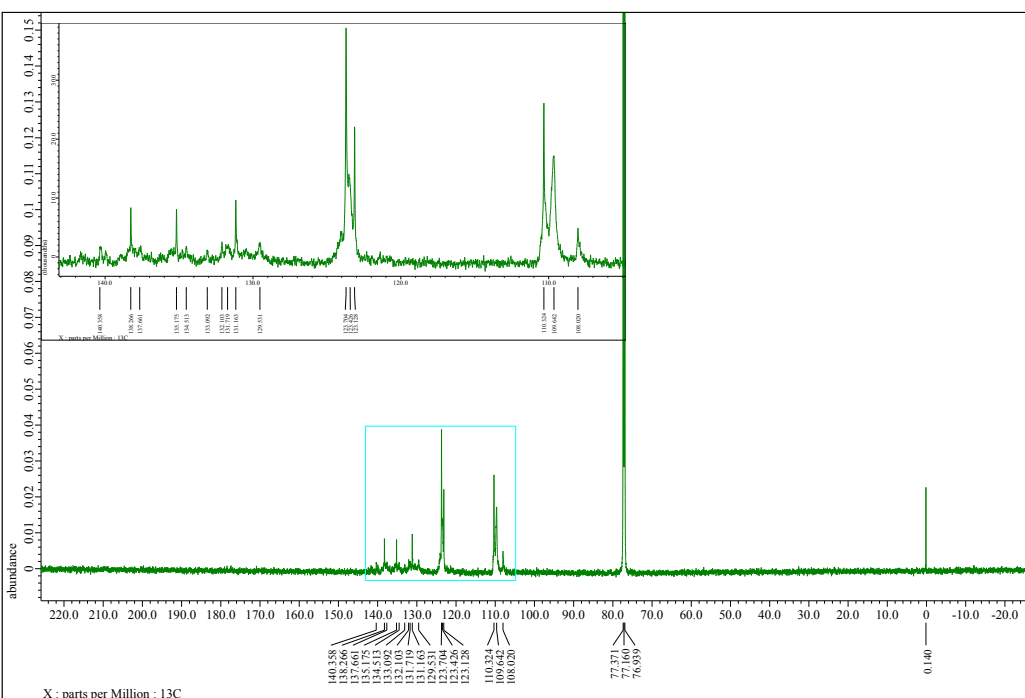


**Fig. S34.**  $^{13}\text{C}\{^1\text{H}\}$  NMR spectrum of **5** (150 MHz,  $\text{CDCl}_3$ ). Reference:  $\text{CDCl}_3$  (77.16 ppm)

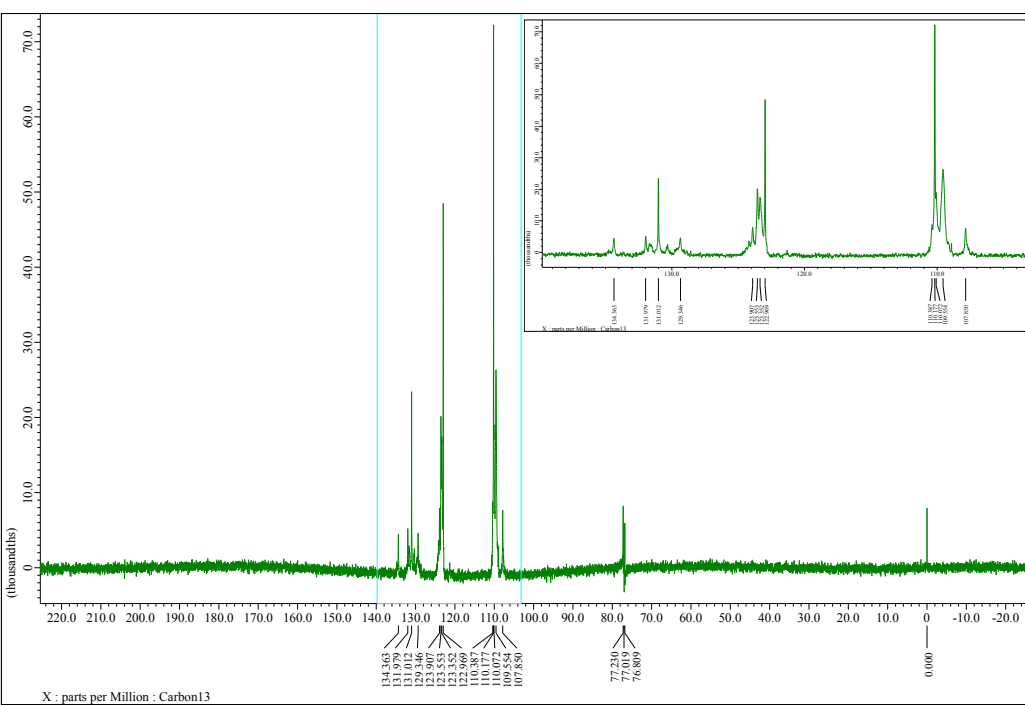


**Fig. S35.**  $^{13}\text{C}\{^1\text{H}\}$  NMR (DEPT-135) spectrum of **5** (150 MHz,  $\text{CDCl}_3$ ). Reference: TMS (0.00 ppm)

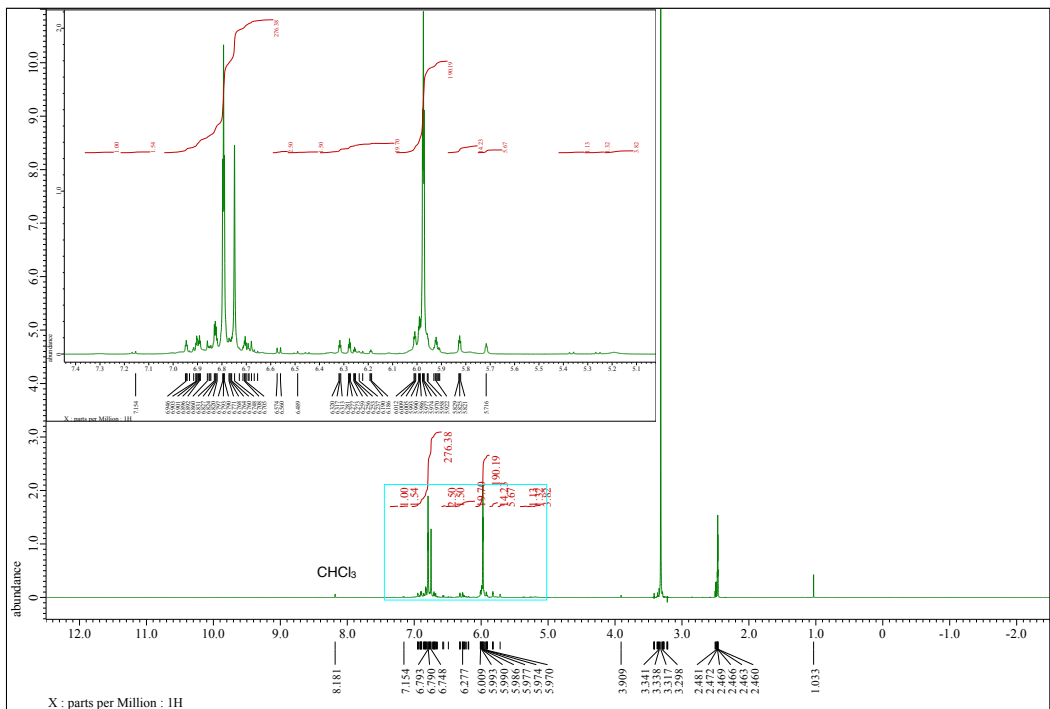


**Fig. S36.**  $^1\text{H}$  NMR spectrum of **5** (600 MHz, DMSO-*d*<sub>6</sub>). Reference: DMSO-*d*<sub>6</sub> (2.50 ppm)

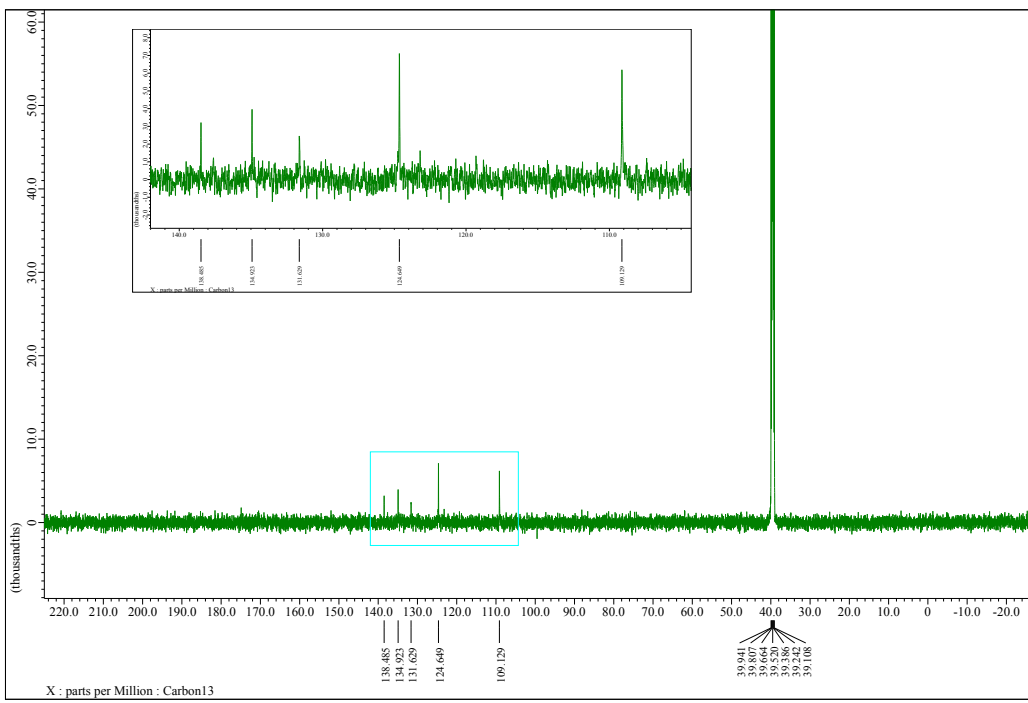


**Fig. S37.**  $^{13}\text{C}\{^1\text{H}\}$  NMR spectrum of **5** (150 MHz, DMSO-*d*<sub>6</sub>). Reference: DMSO-*d*<sub>6</sub> (39.52 ppm)

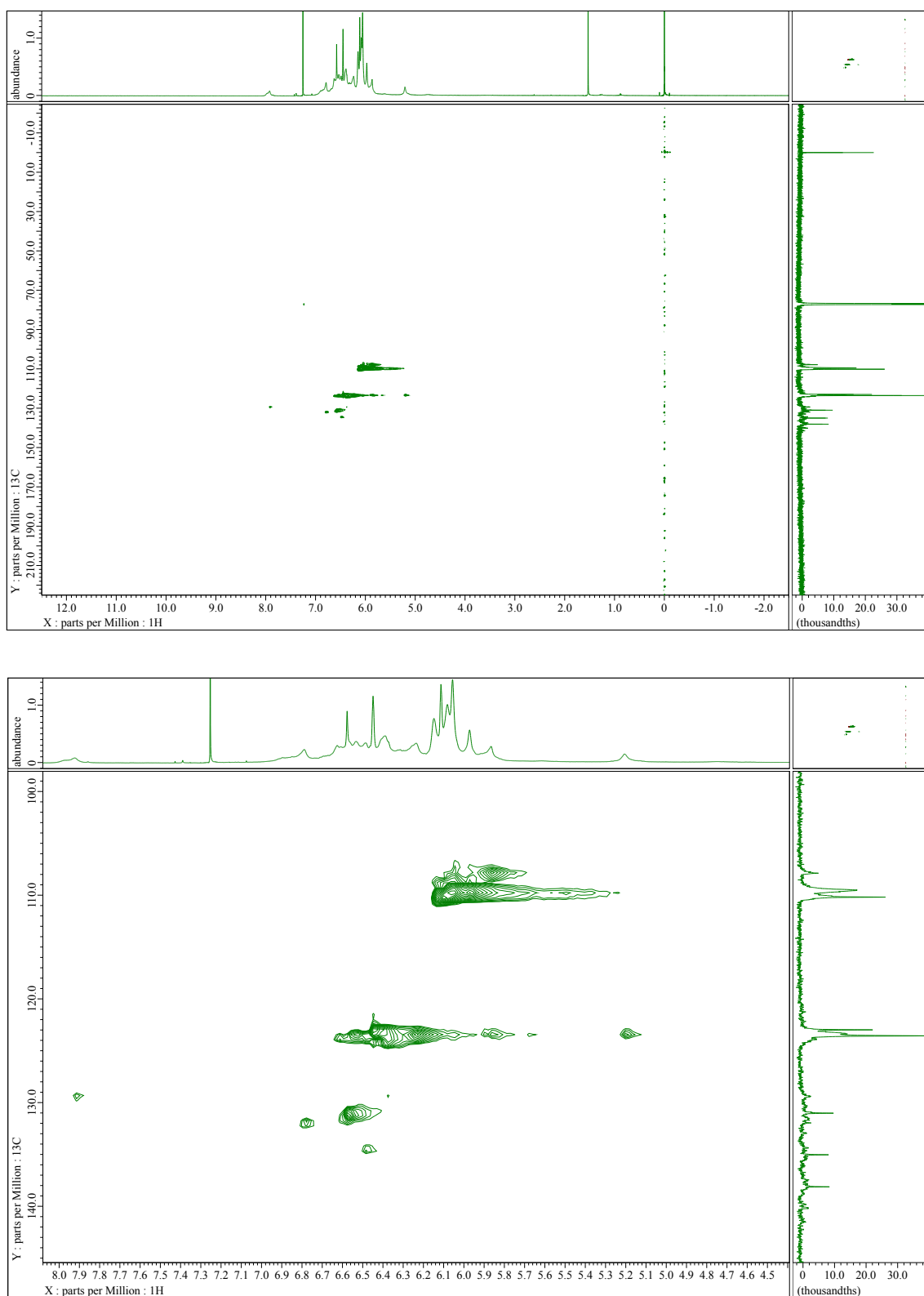


**Fig. S38.**  $^1\text{H}$ - $^{13}\text{C}$  HSQC spectrum of **5** (600 MHz,  $\text{CDCl}_3$ ).

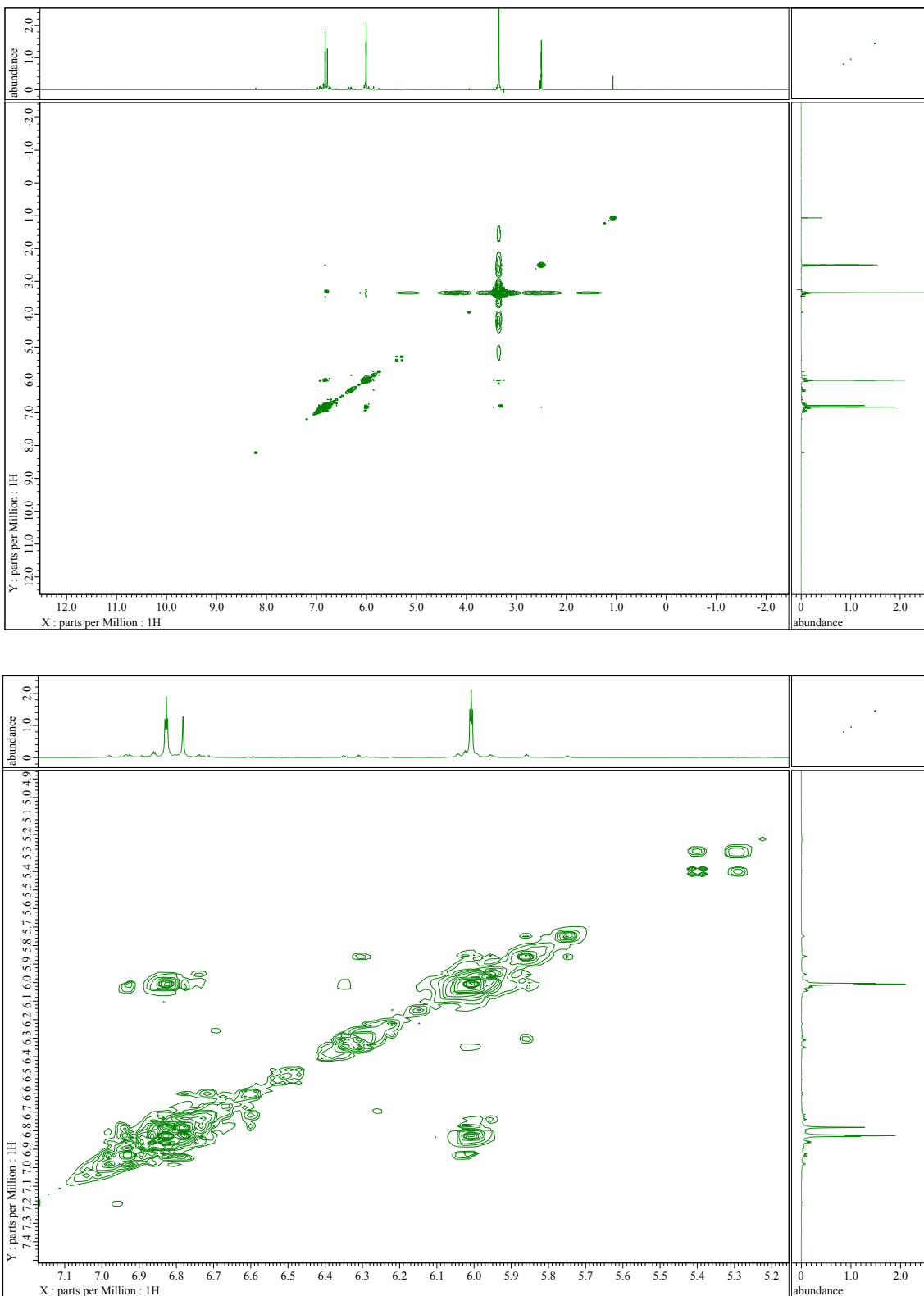


**Fig. S39.**  $^1\text{H}$ - $^1\text{H}$  COSY spectrum of **5** (600 MHz,  $\text{DMSO}-d_6$ ).

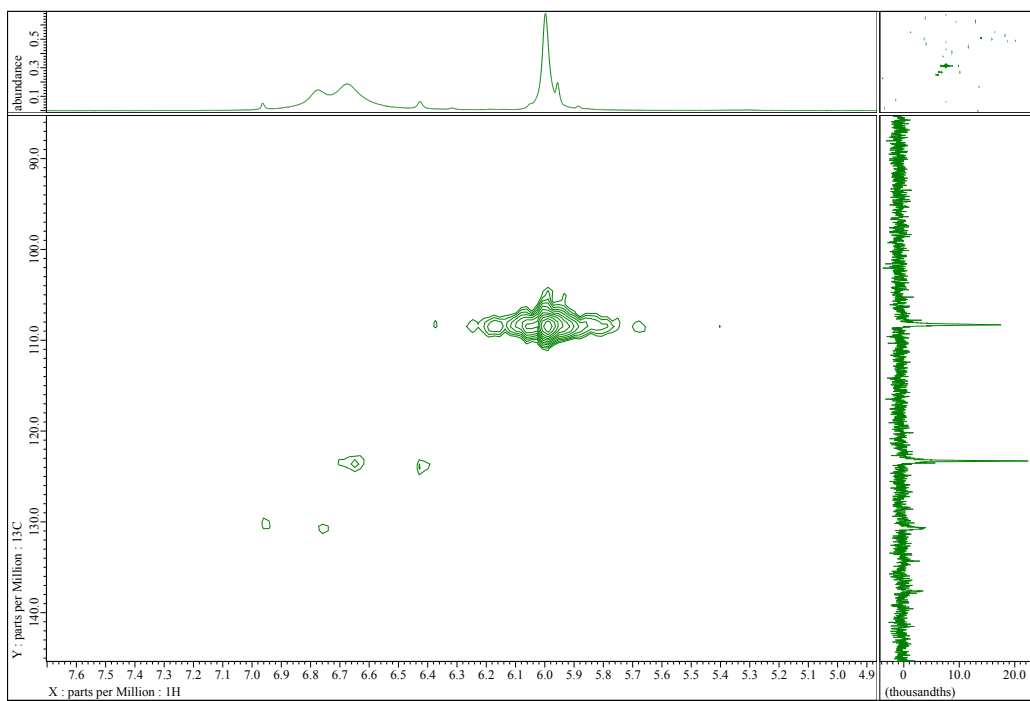


**Fig. S40.**  $^1\text{H}$ - $^{13}\text{C}$  HMQC spectrum of **5** at 150 °C (600 MHz,  $\text{DMSO}-d_6$ ).

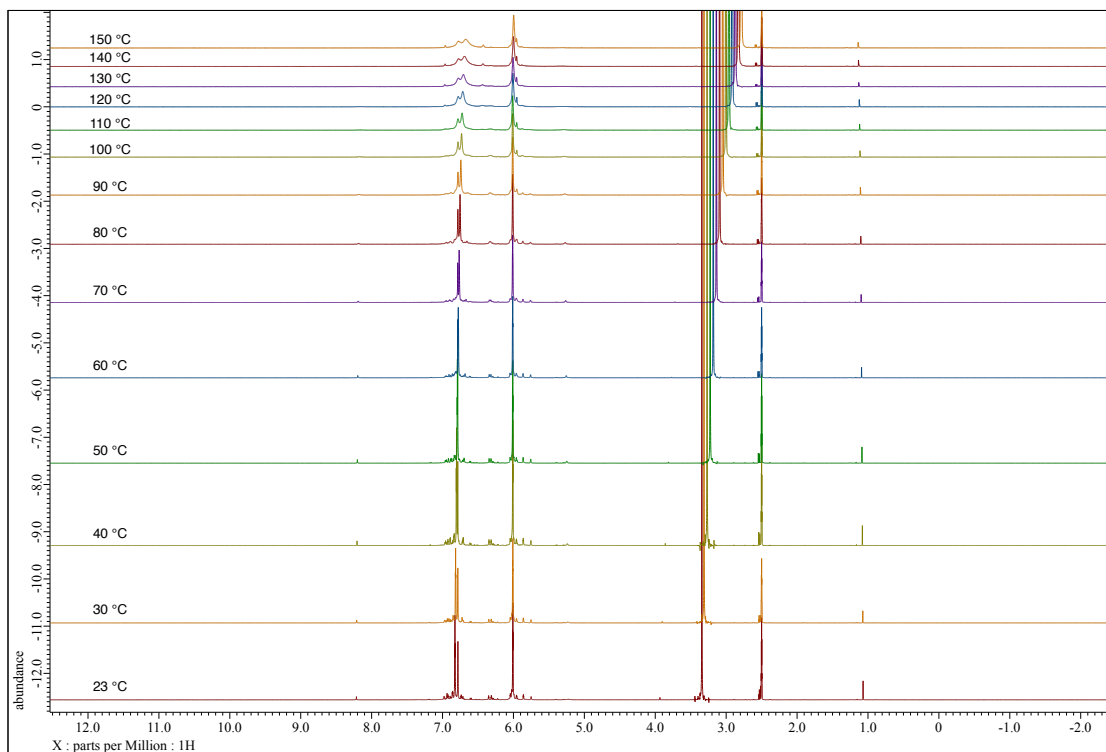


**Fig. S41.**  $^1\text{H}$  VT-NMR overall spectrum of **5** (600 MHz,  $\text{DMSO}-d_6$ ).

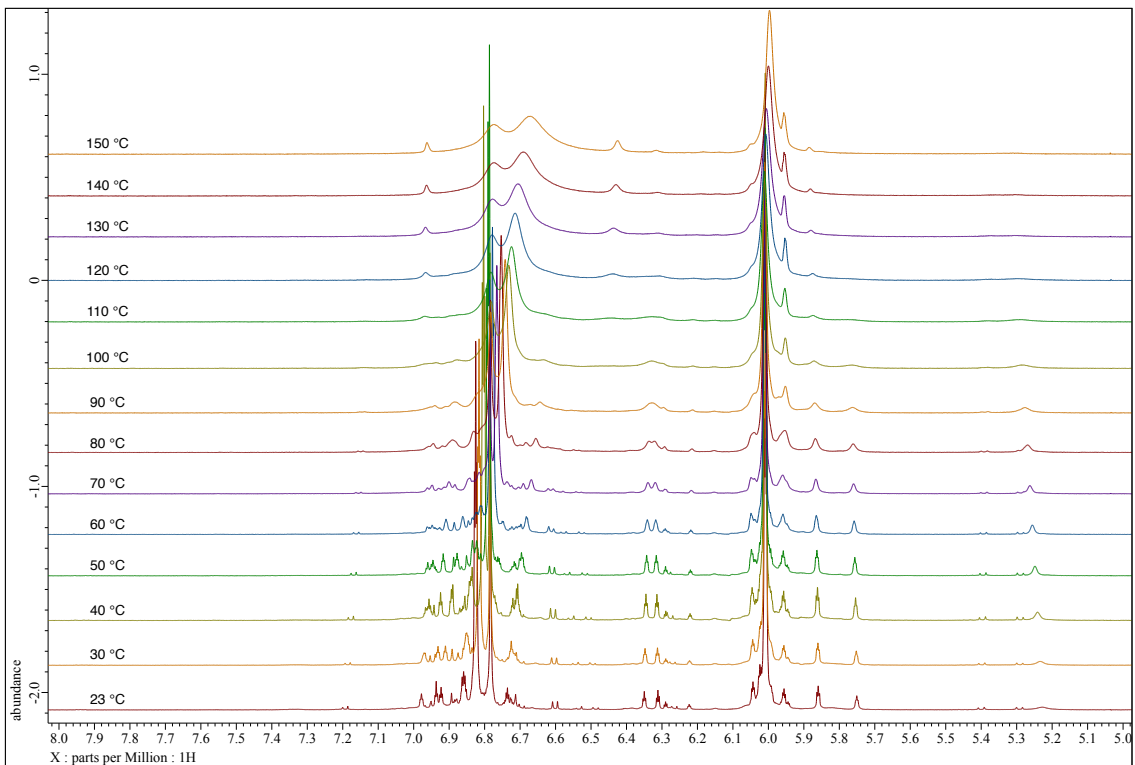
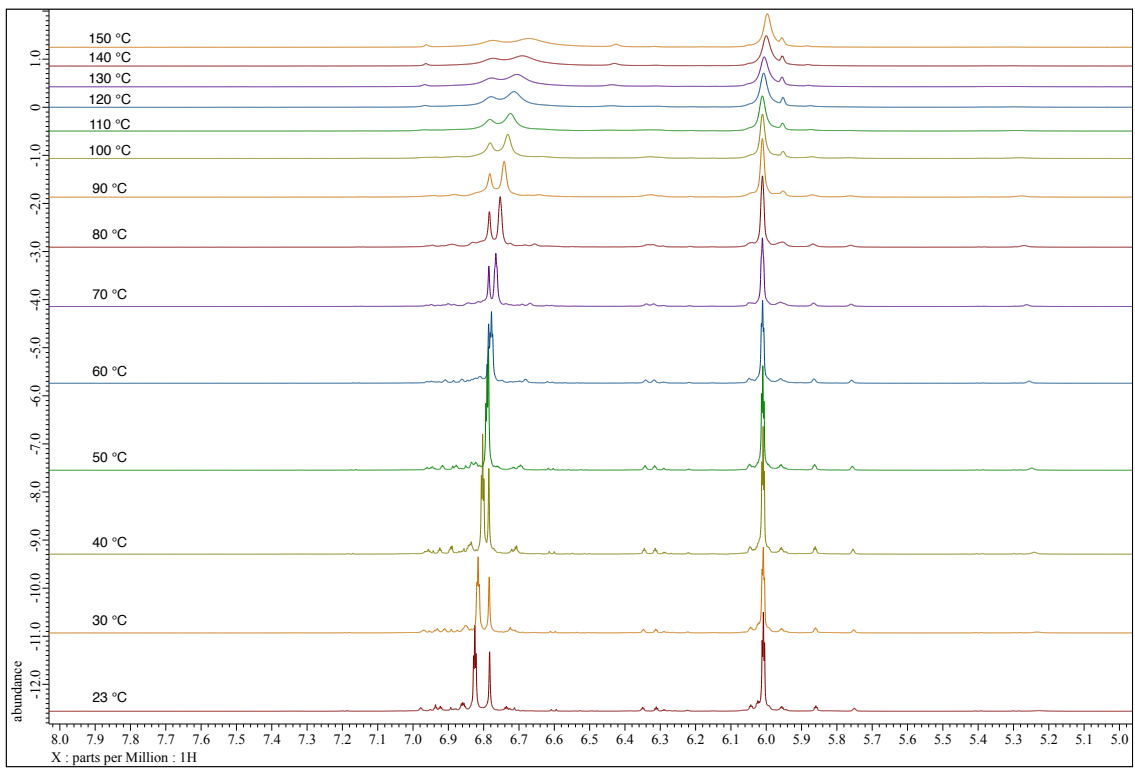


**Fig. S42.**  $^1\text{H}$  VT-NMR spectrum (5.0 ppm–8.0 ppm) of **5** (600 MHz,  $\text{DMSO}-d_6$ ).

## 9. HRMS spectra of 1, 2, and 5

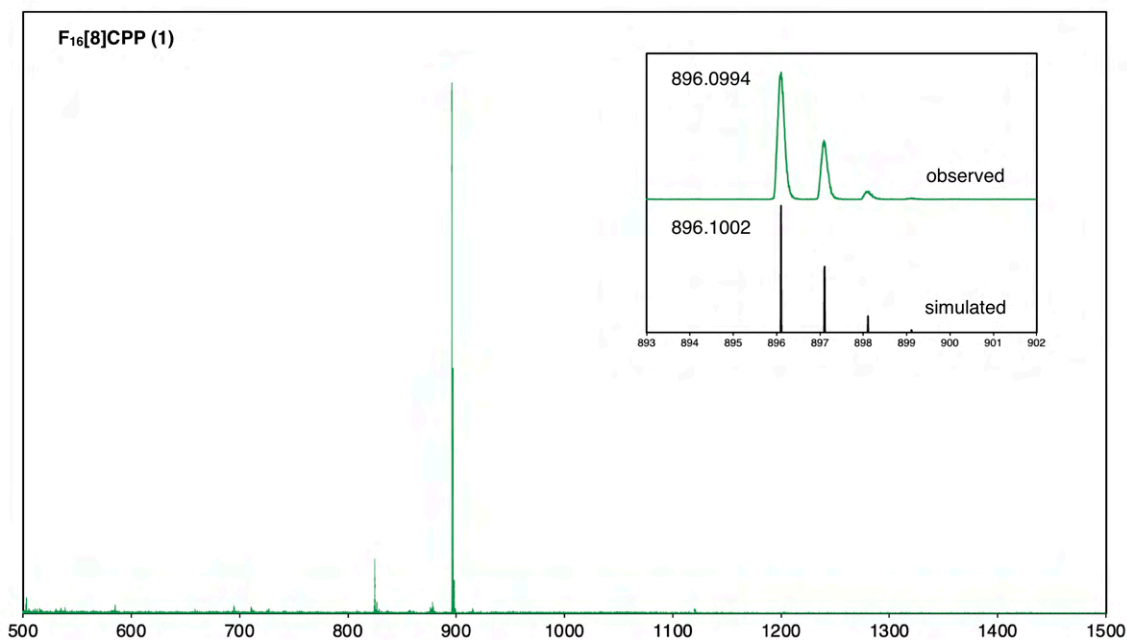


**Fig. S43.** LDI-TOF mass spectrum (spiral NEG mode) of **1**.

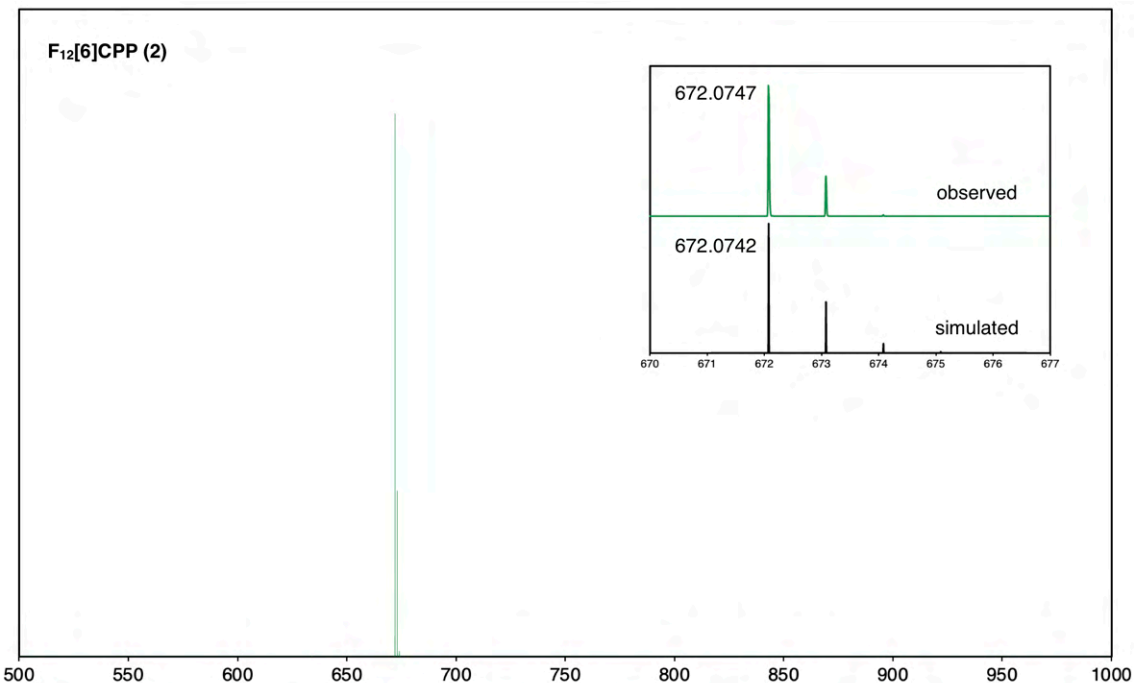


**Fig. S44.** LDI-TOF mass spectrum (spiral POS mode) of **2**.

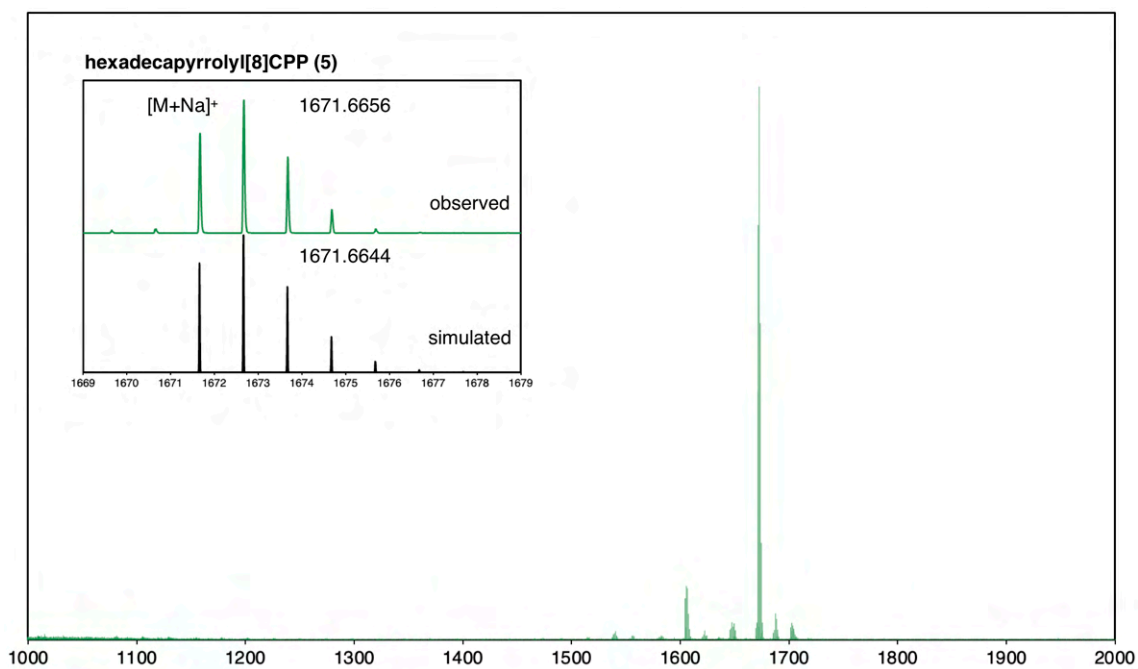


**Fig. S45.** LDI-TOF mass spectrum (spiral POS mode/cationizing agent: NaTFA) of **5**. The other minor peaks are sodium-unadducted peak of **5**, pyrrole fragmented peak (not the unreacted compound), and peaks of oxidized **5**.

## 10. References

- S1 B. Maiti, K. Wang, S. Bhandari, S. D. Bunge, R. J. Twieg and B. D. Dunietz, *J. Mater. Chem. C* 2019, **7**, 3881–3888.
- S2 Y. Tsuchido, R. Abe, T. Ide and K. Osakada, *Angew. Chem., Int. Ed.* 2020, **59**, 22928–22932.
- S3 H. Shudo, M. Kuwayama, M. Shimasaki, T. Nishihara, Y. Takeda, N. Mitoma, T. Kuwabara, A. Yagi, Y. Segawa and K. Itami, *Nat. Commun.* 2022, **13**, 3713.
- S4 G. M. Sheldrick, *Acta Crystallogr.* 2015, **A71**, 3–8.
- S5 G. M. Sheldrick, *Acta Crystallogr.* 2015, **C71**, 3–8.
- S6 O. V. Dolomanov, L. J. Bourhis, R. J. Gildea, J. A. K. Howard and H. Puschmann, *J. Appl. Crystallogr.* 2009, **42**, 339–341.
- S7 S. N. Spisak, Z. Wei, E. Darzi, R. Jasti and M. A. Petrukhina, *Chem. Commun.* 2018, **54**, 7818.
- S8 J. Xia, J. W. Bacon and R. Jasti, *Chem. Sci.* 2012, **3**, 3018–3021.
- S9 M. J. Frisch, G. W. Trucks, H. B. Schlegel, G. E. Scuseria, M. A. Robb, J. R. Cheeseman, G. Scalmani, V. Barone, G. A. Petersson, H. Nakatsuji, X. Li, M. Caricato, A. V. Marenich, J. Bloino, B. G. Janesko, R. Gomperts, B. Mennucci, H. P. Hratchian, J. V. Ortiz, A. F. Izmaylov, J. L. Sonnenberg, D. Williams-Young, F. Ding, F. Lipparini, F. Egidi, J. Goings, B. Peng, A. Petrone, T. Henderson, D. Ranasinghe, V. G. Zakrzewski, J. Gao, N. Rega, G. Zheng, W. Liang, M. Hada, M. Ehara, K. Toyota, R. Fukuda, J. Hasegawa, M. Ishida, T. Nakajima, Y. Honda, O. Kitao, H. Nakai, T. Vreven, K. Throssell, J. A. Montgomery, Jr., J. E. Peralta, F. Ogliaro, M. J. Bearpark, J. J. Heyd, E. N. Brothers, K. N. Kudin, V. N. Staroverov, T. A. Keith, R. Kobayashi, J. Normand, K. Raghavachari, A. P. Rendell, J. C. Burant, S. S. Iyengar, J. Tomasi, M. Cossi, J. M. Millam, M. Klene, C. Adamo, R. Cammi, J. W. Ochterski, R. L. Martin, K. Morokuma, O. Farkas, J. B. Foresman and D. J. Fox, Gaussian 16, Revision C.01, Gaussian, Inc., Wallingford CT, 2016.
- S10 A. D. Becke, *J. Chem. Phys.* 1993, **98**, 5648–5652.
- S11 C. Lee, W. Yang and R. G. Parr, *Phys. Rev. B* 1988, **37**, 785–789.
- S12 E. R. Johnson, S. Keinan, P. Mori-Sánchez, J. Contreras-García, A. J. Cohen, W. Yang, *J. Am. Chem. Soc.* 2010, **132**, 6498.
- S13 J. Contreras-García, E. R. Johnson, S. Keinan, R. Chaudret, J. P. Piquemal, D. N. Beratan, W. Yang, *J. Chem. Theory Comput.* 2011, **7**, 625.